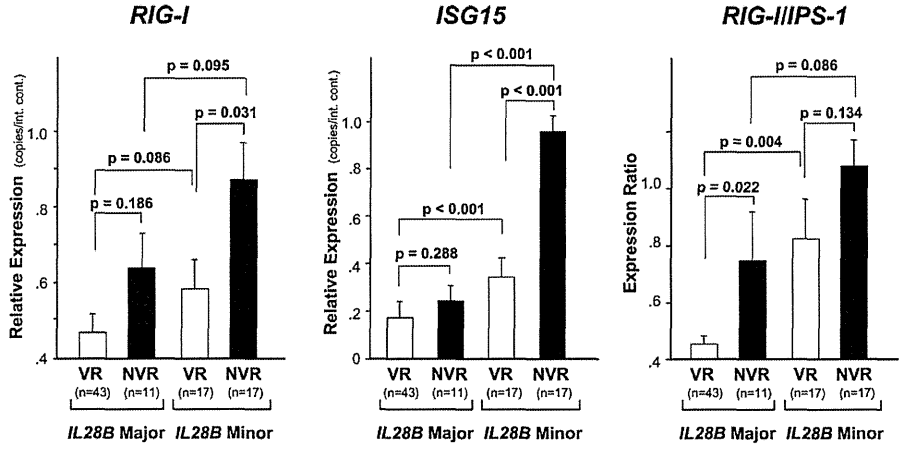

Fig. 3. Comparison of hepatic gene expression levels between virological responders (VR) and nonvirological responders (NVR) in subgroups of the *IL28B* genotype (*IL28B* Major, rs8099917 TT/rs12979860 CC; *IL28B* Minor, rs8099917 TG/rs12979860 CT). Expressions of *RIG-I* and *ISG15* as well as the *RIG-I/IPS-1* expression ratio are shown. Error bars indicate standard error. The numbers of patients in each subgroup are shown in the bottom of the figure.

prediction of NVR (Table 2). The area under the ROC curve for *IL28B* genotype was 0.662, which was lower compared with that for *RIG-I* and *ISG15* expressions and *RIG-I/IPS-1* ratio.

When we stratified the patients by the cutoff value for *RIG-I* and *ISG15* expressions and *RIGI/IPS-1* ratio, no statistically significant difference was found in NVR rates among *IL28B* genotypes within the same subgroup (Fig. 4B).

Factors Associated with NVR. In univariate analysis, age, platelet counts, double mutation at amino acid positions 70 and 91 of the HCV core region, *IL28B* minor allele, and hepatic expressions of *RIG-I, MDA5, LGP2, ISG15*, and *USP18*, and *RIG-I/IPS-1* ratio were significantly

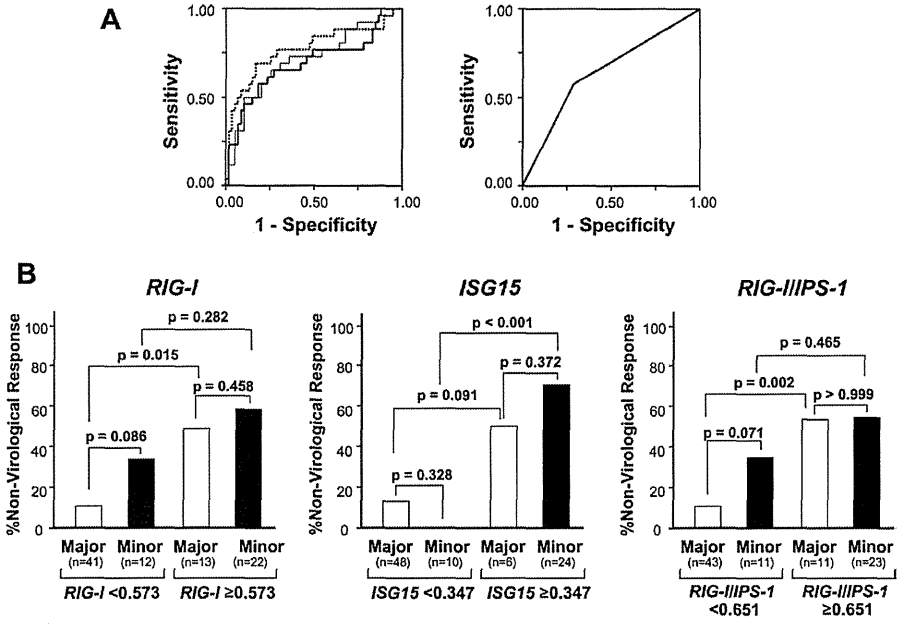

Fig. 4. (A) Receiver operator characteristics (ROC) curve for prediction of nonvirological response. ROC curves were generated to compare *RIG-I* (black line), *ISG15* (dotted line), and *RIG-I/IPS-1* ratio (gray line) (all in the left panel), and *IL28B* genotype (in the right panel). (B) Nonvirological response rate in *IL28B* major (rs8099917 TT/rs12979860 CC) and minor patients (rs8099917 TG/rs12979860 CT) in subgroups divided by the cutoff value of *RIG-I* and *ISG15* expression and the *RIG-I/ISG15* ratio determined by ROC analysis. Cutoff values of *RIG-I* and *ISG15* expression are expressed as expression copy number normalized to the expression of an internal control. The numbers of patients in each subgroup are shown in the bottom of the figure.

Table 2. Area Under the ROC Curves, Sensitivity, Specificity, and Negative as Well as Positive Predictive Values of Nonvirological Responses

Variables	AUC	95% CI	Cutoff	Sensitivity	Specificity	NPV	PPV
RIG-I (copies/int. control)	0.712	0.584-0.840	0.573	0.679	0.733	0.830	0.543
ISG15 (copies/int. control)	0.782	0.666-0.899	0.347	0.714	0.833	0.862	0.667
RIG-I/IPS-1 (copies/int. control)	0.732	0.611-0.852	0.651	0.679	0.750	0.833	0.559
IL28B genotype	0.662	0.537-0.787	TG*/CT†	0.607	0.717	0.796	0.500

AUC, area under the curve; NPV, negative predictive value; PPV, positive predictive value.
*Genotype at rs8099917.
†Genotype at rs12979860.

associated with NVR (Table 3). Among these, multivariate analysis identified old age, HCV core double mutant, and higher hepatic expressions of *RIG-I* and *ISG15* as factors independently associated with NVR (Table 3).

IPS-1 and RIG-I Protein Expression in the Liver. Western blotting revealed that full-length and cleaved IPS-1 were variably present in all the samples from CH-C patients (Fig. 5A). Similar to mRNA

Table 3. Factors Associated with Nonvirological Response

	Univariate Analysis		Multivariate Analysis*	
Factors	Risk Ratio (95% CI)	*P*-value	Risk Ratio (95% CI)	*P*-value
Age (by every 10 year)	1.84 (1.10-3.14)	0.027	3.76 (1.19-11.7)	0.023
Sex				
Male	1			
Female	1.62 (0.59-4.42)	0.350		
BMI (by every 5 kg/m^2)	0.87 (0.46-1.65)	0.672		
Fibrosis stage				
F1/F2	1			
F3/F4	1.82 (0.69-4.85)	0.228		
Degree of steatosis				
<10%	1			
≥10%	1.46 (0.43-5.03)	0.544		
Albumin (by every 1 g/dL)	0.41 (0.11-1.56)	0.190		
AST (by every 40 IU/L)	0.89 (0.53-1.56)	0.681		
ALT (by every 40 IU/L)	0.85 (0.57-1.32)	0.481		
γ-GTP (by every 40 IU/L)	1.32 (0.82-2.07)	0.235		
Fasting blood sugar (by every 100 mg/dL)	1.35 (0.74-2.45)	0.340		
Hemoglobin (by every 1 g/dL)	0.93 (0.67-1.31)	0.683		
Platelet counts (by every 10^4/μL)	0.90 (0.82-0.99)	0.037	0.92 (0.78-1.08)	0.296
HCV load (by every 100 KIU/mL)	1.00 (1.00-1.00)	0.688		
Core 70 & 91 double mutation				
Wild	1		1	
Mutant	3.92 (1.14-13.5)	0.030	11.1 (1.40-88.7)	0.023
ISDR				
Nonwildtype	1			
Wildtype	1.38 (0.13-3.61)	0.513		
IL28B genotype				
Major allele†	1		1	
Minor allele‡	3.91 (1.52-10.0)	0.005	1.53 (0.20-11.9)	0.684
Hepatic gene expression (by every 0.1 copy/*int. control*)				
RIG-I	1.28 (1.10-1.50)	0.002	1.53 (1.07-2.22)	0.021
MDA5	1.53 (1.12-2.00)	0.001		
LGP2	1.34 (1.04-1.74)	0.026		
IPS-1	0.90 (0.78-1.04)	0.143		
RNF125	0.93 (0.83-1.04)	0.204		
ISG15	1.37 (1.16-1.62)	<0.001	1.28 (1.04-1.58)	0.021
USP18	1.67 (1.27-2.20)	<0.001		
IFNλ	1.02 (0.99-1.05)	0.170		
RIG-I/IPS-1 ratio (by every 0.1)	1.21 (1.07-1.36)	0.002		

Risk ratios for nonvirological response were calculated by the logistic regression analysis. BMI, body mass index; AST, aspartate aminotransferase; ALT, alanine aminotransferase; γ-GTP, gamma-glutamyl transpeptidase; HCV, hepatitis C virus; ISDR, IFN sensitivity determining region.
*Multivariate analysis was performed with factors significantly associated with nonvirological response by univariate analysis except for *MDA5*, *LGP2*, *USP18*, and *RIG-I/IPS-1* ratio, which were significantly correlated with *RIG-I* and *ISG15*.
†rs8099917 TT and rs12979860 CC.
‡rs8099917 TG and rs12979860 CT.

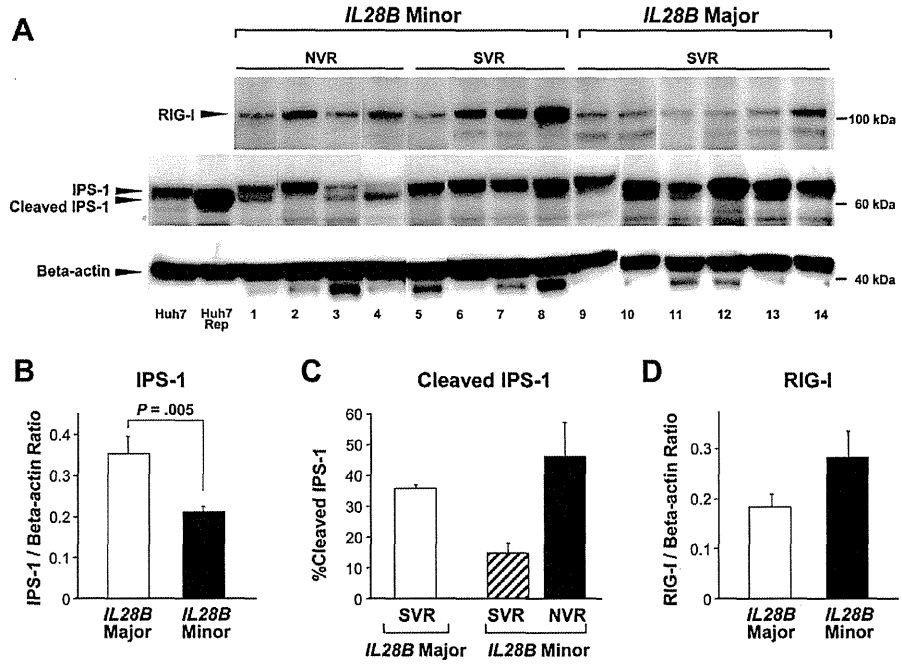

Fig. 5. (A) Western blotting for IPS-1 and RIG-I protein expression levels. Eight lanes contain samples from *IL28B* minor patients (lanes 1-8) and six lanes contain samples from *IL28B* major patients (lanes 9-14). Four lanes contain samples from nonvirological responders (NVR, lanes 1-4) and 10 lanes contain samples from sustained virological responders (SVR, lanes 5-14). Specific bands for RIG-I, full-length IPS-1, cleaved IPS-1, and β-actin are indicated by arrows. Naive Huh7 cells were used for a positive control for full-length IPS-1 (lane Huh7), and cells transfected with HCV-1b subgenomic replicon (Reference #20) were used for a positive control for cleaved IPS-1 (lane Huh7 Rep). (B) Total IPS-1 protein expression levels normalized to β-actin according to *IL28B* genotype. Error bars indicate standard error. *P*-value was determined by Mann-Whitney *U* test. (C) Percentage of cleaved IPS-1 products in total IPS-1 protein according to treatment responses stratified by *IL28B* genotype. Error bars indicate standard error. (D) RIG-I protein expression levels normalized to β-actin according to *IL28B* genotype. Error bars indicate standard error.

expression, total hepatic IPS-1 protein expression was significantly lower in *IL28B* minor patients than in *IL28B* major patients (Fig. 5B). With regard to *IL28B* minor patients, the percentage of cleaved IPS-1 protein in total IPS-1 in SVR was lower than that in NVR (Fig. 5C). In contrast to IPS-1 protein expression, hepatic RIG-I protein expression was higher in *IL28B* minor patients than that in *IL28B* major patients (Fig. 5D).

Discussion

In the present study we found that the baseline expression levels of intrahepatic viral sensors and related regulatory molecules were significantly associated with the genetic variation of *IL28B* and final virological outcome in CH-C patients treated with PEG-IFNα/RBV combination therapy. Although the relationship between the *IL28B* minor allele and NVR in PEG-IFNα/RBV combination therapy is evident, mechanisms responsible for this association remain unknown. *In vitro* studies have suggested that cytoplasmic viral sensors, such as RIG-I and MDA5, play a pivotal role in the regulation of IFN production and augment IFN production through an amplification circuit.[7,8] Our results indicate that expressions of *RIG-I* and *MDA5* and a related amplification system may be up-regulated by endogenous IFN at a higher baseline level in *IL28B* minor patients. However, HCV elimination by subsequent exogenous IFN is insufficient in these patients, as reported,[19] suggesting that *IL28B* minor patients may have adopted a different equilibrium in their innate immune response to HCV. Our data are further supported by recent reports of an association between intrahepatic levels of IFN-stimulated gene expression and PEG-IFNα/RBV response as well as with *IL28B* genotype.[21-23]

In contrast to cytoplasmic viral sensor (*RIG-I, MDA5*, and *LGP2*) and modulator (*ISG15* and *USP18*) expression, the adaptor molecule (*IPS-1*) expression was significantly lower in *IL28B* minor patients. Moreover, western blotting further confirmed IPS-1 protein downregulation in *IL28B* minor patients by revealing decreased protein levels. Because IPS-1 is one of the main target molecules of HCV evasion,[9,18]

transcriptional and translational *IPS-1* expression are probably suppressed by HCV with resistant phenotype, which may be more adaptive in *IL28B* minor patients than in *IL28B* major patients. When we analyzed the proportion of full-length or cleaved IPS-1 to the total IPS-1 protein in a subgroup of *IL28B* minor patients, cleaved IPS-1 product was less dominant in SVR than in NVR, whereas uncleaved full-length IPS-1 protein was more dominant in SVR than in NVR. Therefore, the ability of HCV to evade host innate immunity by cleaving IPS-1 protein and/or host capability of protection from IPS-1 cleavage is probably responsible for the variable treatment responses in *IL28B* minor patients.

Our results indicated a close association between *IL28B* minor patients with higher γ-GTP level and higher frequency of HCV core double mutants, which are known factors for NVR. In contrast, no significant association was observed between *IL28B* genotype and age, gender, or liver fibrosis, which are also known to be unfavorable factors for virological response to PEG-IFNα/RBV. Therefore, certain factors other than the *IL28B* genotype may independently influence virological response. To elucidate whether gene expression involving innate immunity independently associates with a virological response from the *IL28B* genotype, we performed further analysis in a subgroup and conducted a multivariate regression and ROC analyses. Our multivariate and ROC analyses demonstrate that higher expressions of *RIG-I* and *ISG15* as well as a higher ratio of *RIG-I/IPS-1* are independently associated with NVR, and quantification of these values is more useful in predicting final virological response to PEG-IFNα/RBV than determination of *IL28B* genotype in each individual patients. However, the SVR rates in our patients were similar among *IL28B* genotypes, which suggests more SVR patients with the *IL28B* minor allele were included in the present study than those in the general CH-C population. Hence, our data did not necessarily exclude the possibility of the *IL28B* genotype in predicting NVR, although our multivariate analysis could not identify the *IL28B* minor allele as an independent factor for NVR. Interestingly, an association between *IL28B* genotype and expressions of *RIG-I* and *ISG15* as well as *RIG-I/IPS-1* expression ratio is still observed even in patients with the same subgroup of virological response (Fig. 3).

In the present study, although hepatic *IFNλ* expression was observed to be higher in *IL28B* minor and NVR patients, it was not statistically significant. Because *IL28B* shares 98.2% homology with *IL28A*, our primer could not distinguish the expression of *IL28B* from that of *IL28A*, and moreover, we could not specify which cell expresses *IFNλ* (i.e., hepatocytes or other immune cells that have infiltrated the liver). Therefore, the precise mechanisms underlying *IL28B* variation and expression of *IFNλ* in relation to treatment response need further clarification by specifying type of IFNλ and uncovering the producing cells.

In the present study we included genotype 1b patients because it is imperative to designate a virologically homogenous patient group to associate individual treatment responses with different gene expression profiles that direct innate immune responses. We have reported that the *RIG-I/IPS-1* ratio was significantly higher in NVR with HCV genotype 2.[19] However, our preliminary results indicated that baseline hepatic *RIG-I* and *ISG15* expression and the *RIG-I/IPS-1* expression ratio is not significantly different among *IL28B* genotypes in patients infected with genotype 2 (Supporting Figure). This may be related to the rarity of NVR with HCV genotype 2 and the lower effect of *IL28B* genotype on virological responses in patients infected with HCV genotype 2.[24] The association among treatment responses in all genotypes, the different status of innate immune responses, and *IL28B* genotype needs to be examined further.

Differences in allele frequency for *IL28B* SNPs among the population groups has been reported. The frequency of *IL28B* major allele among patients with Asian ancestry is higher than that among patients with European and African ancestry.[25] Because *IL28B* polymorphism strongly influences treatment responses within each population group,[5] our data obtained from Japanese patients can be applied to other population groups. However, the rate of SVR having African ancestry was lower than that having European ancestry within the same *IL28B* genotype.[5] Hence, further study is required to clarify whether this difference among the population groups with the same *IL28B* genotype could be explained by differences in expression of genes involved in innate immunity.

In a recent report, an SVR rate of telaprevir with PEG-IFNα/RBV was only 27.6% in *IL28B* minor patients.[26] Because new anti-HCV therapy should still contain PEG-IFNα/RBV as a platform for the therapy, our findings regarding innate immunity in addressing the mechanism of virological response and predicting NVR remain important in this new era of directly acting anti-HCV agents, such as telaprevir and boceprevir.

In conclusion, this clinical study in humans demonstrates the potential relevance of the molecules involved in innate immunity to the genetic variation

of *IL28B* and clinical response to PEG-IFNα/RBV. Both the *IL28B* minor allele and higher expressions of *RIG-I* and *ISG15* as well as higher *RIG-I/IPS-1* ratio are independently associated with NVR. Innate immune responses in *IL28B* minor patients may have adapted to a different equilibrium compared with that in *IL28B* major patients. Our data will advance both understanding of the pathogenesis of HCV resistance and the development of new antiviral therapy targeted toward the innate immune system.

References

1. Kiyosawa K, Sodeyama T, Tanaka E, Gibo Y, Yoshizawa K, Nakano Y, et al. Interrelationship of blood transfusion, non-A, non-B hepatitis and hepatocellular carcinoma: analysis by detection of antibody to hepatitis C virus. HEPATOLOGY 1990;12:671-675.
2. Zeuzem S, Pawlotsky JM, Lukasiewicz E, von Wagner M, Goulis I, Lurie Y, et al. DITTO-HCV Study Group. International, multicenter, randomized, controlled study comparing dynamically individualized versus standard treatment in patients with chronic hepatitis C. J Hepatol 2005;43:250-257.
3. Tanaka Y, Nishida N, Sugiyama M, Kurosaki M, Matsuura K, Sakamoto N, et al. Genome-wide association of IL28B with response to pegylated IFN-alpha and ribavirin therapy for chronic hepatitis C. Nat Genet 2009;10:1105-1109.
4. Suppiah V, Moldovan M, Ahlenstiel G, Berg T, Weltman M, Abate ML, et al. IL28B is associated with response to chronic hepatitis C IFN-alpha and ribavirin therapy. Nat Genet 2009;10:1100-1104.
5. Ge D, Fellay J, Thompson AJ, Simon JS, Shianna KV, Urban TJ, et al. Genetic variation in IL28B predicts hepatitis C treatment-induced viral clearance. Nature 2009;461:399-401.
6. Biron CA. Initial and innate responses to viral infections—pattern setting in immunity or disease. Curr Opin Microbiol 1999;2:374-381.
7. Yoneyama M, Kikuchi M, Natsukawa T, Shinobu N, Imaizumi T, Miyagishi M, et al. The RNA helicase RIG-I has an essential function in double-stranded RNA-induced innate antiviral responses. Nat Immunol 2004;5:730-737.
8. Yoneyama M, Kikuchi M, Matsumoto K, Imaizumi T, Miyagishi M, Taira K, et al. Shared and unique functions of the DExD/H-box helicases RIG-I, MDA5, and LGP2 in antiviral innate immunity. J Immunol 2005;175:2851-2858.
9. Meylan E, Curran J, Hofmann K, Moradpour D, Binder M, Bartenschlager R, et al. Cardif is an adaptor protein in the RIG-I antiviral pathway and is targeted by hepatitis C virus. Nature 2005;437: 1167-1172.
10. Kawai T, Takahashi K, Sato S, Coban C, Kumar H, Kato H, et al. IPS-1, an adaptor triggering RIG-I- and Mda5-mediated type I interferon induction. Nat Immunol 2005;6:981-988.
11. Seth RB, Sun L, Ea CK, Chen ZJ. Identification and characterization of MAVS, a mitochondrial antiviral signaling protein that activates NF-kappaB and IRF 3. Cell 2005;122:669-682.
12. Xu LG, Wang YY, Han KJ, Li LY, Zhai Z, Shu HB. VISA is an adapter protein required for virus-triggered IFN-beta signaling. Mol Cell 2005;19:727-740.
13. Rothenfusser S, Goutagny N, DiPerna G, Gong M, Monks BG, Schoenemeyer A, et al. The RNA helicase Lgp2 inhibits TLR-independent sensing of viral replication by retinoic acid-inducible gene-I. J Immunol 2005;175:5260-5268.
14. Arimoto K, Takahashi H, Hishiki T, Konishi H, Fujita T, Shimotohno K. Negative regulation of the RIG-I signaling by the ubiquitin ligase RNF125. Proc Natl Acad Sci U S A 2007;104:7500-7505.
15. Zhao C, Denison C, Huibregtse JM, Gygi S, Krug RM. Human ISG15 conjugation targets both IFN-induced and constitutively expressed proteins functioning in diverse cellular pathways. Proc Natl Acad Sci U S A 2005;102:10200-10205.
16. Schwer H, Liu LQ, Zhou L, Little MT, Pan Z, Hetherington CJ, et al. Cloning and characterization of a novel human ubiquitin-specific protease, a homologue of murine UBP43 (Usp18). Genomics 2000;65: 44-52.
17. Malakhov MP, Malakhova OA, Kim KI, Ritchie KJ, Zhang DE. UBP43 (USP18) specifically removes ISG15 from conjugated proteins. J Biol Chem 2002;277:9976-9981.
18. Li XD, Sun L, Seth RB, Pineda G, Chen ZJ. Hepatitis C virus protease NS3/4A cleaves mitochondrial antiviral signaling protein off the mitochondria to evade innate immunity. Proc Natl Acad Sci U S A 2005; 102:17717-17722.
19. Asahina Y, Izumi N, Hirayama I, Tanaka T, Sato M, Yasui Y, et al. Potential relevance of cytoplasmic viral sensors and related regulators involving innate immunity in antiviral response. Gastroenterology 2008;134:1396-1405.
20. Tanabe Y, Sakamoto N, Enomoto N, Kurosaki M, Ueda E, Maekawa S, et al. Synergistic inhibition of intracellular hepatitis C virus replication by combination of ribavirin and interferon-alpha. J Infect Dis 2004;189:1129-1139.
21. Honda M, Sakai A, Yamashita T, Nakamoto Y, Mizukoshi E, Sakai Y, et al. Hepatic ISG expression is associated with genetic variation in interleukin 28B and the outcome of IFN therapy for chronic hepatitis C. Gastroenterology 2010;139:499-509.
22. Urban TJ, Thompson AJ, Bradric SS, Fellay J, Schuppan D, Cronin KD, et al. *IL28B* genotype is associated with differential expression of intrahepatic interferon-stimulated genes in patients with chronic hepatitis C. HEPATOLOGY 2010;52:1888-1896.
23. Dill MT, Duong FHT, Vogt JE, Bibert S, Bochud PY, Terracciano L, et al. Interferon-induced gene expression is a stronger predictor of treatment response than *IL28B* genotype in patients with hepatitis C. Gastroenterology 2011;140:1021-1031.
24. Yu ML, Huang CF, Huang JF, Chang NC, Yang JF, Lin ZY, et al. Role of interleukin-28B polymorphism in the treatment of hepatitis C virus genotype 2 infection in Asian patients. HEPATOLOGY 2011;53:7-13.
25. Thomas DL, Thio CL, Martin MP, Qi Y, Ge D, O'hUigin C, Kidd J, et al. Genetic variation in *IL28B* and spontaneous clearance of hepatitis C virus. Nature 2009;461:798-802.
26. Akuta N, Suzuki F, Hirakawa M, Kawamura Y, Yatsuji H, Sezaki H, et al. Amino acid substitution in hepatitis C virus core region and genetic variation near the interleukin 28B gene predict viral response to teraprevir with pegIFN and ribavirin. HEPATOLOGY 2010;52:421-429.

Biochemical and Biophysical Research Communications 428 (2012) 36–43

Contents lists available at SciVerse ScienceDirect

Biochemical and Biophysical Research Communications

journal homepage: www.elsevier.com/locate/ybbrc

Association of changes in the gene expression profile of blood cells with the local tumor inflammatory response in a murine tumor model

Yoshio Sakai [a,b], Isamu Tatsumi [c], Mami Higashimoto [c], Akihiro Seki [c], Alessandro Nasti [c], Keiko Yoshida [c], Kazunori Kawaguchi [c], Takashi Wada [b], Masao Honda [c], Takuya Komura [c], Shuichi Kaneko [a,c,*]

[a] Department of Gastroenterology, Kanazawa University, Japan
[b] Department of Laboratory Medicine, Kanazawa University, Japan
[c] Disease Control and Homeostasis, Kanazawa University, Japan

ARTICLE INFO

Article history:
Received 28 September 2012
Available online 9 October 2012

Keywords:
Peripheral blood cell
Gene expression profile
Local tumor inflammation

ABSTRACT

Cancer tissue is frequently associated with the host inflammatory response, which involves blood cells. Using DNA microarrays, we examined the gene expression profiles of blood and tumors in a murine subcutaneous hepatocellular carcinoma model, in which tumors develop during the initial 10 days and then diminish and disappear by day 25 after implantation. Immunohistochemical and gene expression analysis indicated that tumor tissues were associated with an active immune response, particularly the CD4+ T cell-mediated immune response, on day 10. The genes commonly up-regulated in blood and the fraction enriched with tumor-associated inflammatory cells on day 10 also suggested the involvement of CD4+ T cells. Unsupervised hierarchical clustering analysis of gene expression of peripheral blood cells on days 0, 10, 15, 20, and 25 indicated two major clusters: the tumor-existence cluster on days 10, 15, and 20, and the tumor-free cluster on days 0 and 25. Additionally, sub-clusters were detected on each day. These results suggest that the gene expression profile of whole blood cells is affected by the local tumor condition, and is associated with the local host immune response. Its analysis will facilitate exploration of the underlying important features of the host immune response to tumors.

1. Introduction

Cancer is one of the most serious diseases if early diagnosis fails or in cases of recurrence after radical treatment [1]. Therefore, elucidating the detailed biological features of cancer is important for development of new useful diagnostic and therapeutic methods to improve the prognosis of cancer patients [2]. Immunity is an important physiological homeostasis system that protects the host from various diseases. Cancer is frequently associated with the immune reaction of the host [3], although cancer originates from self tissues. Peripheral blood contains a substantial number of immune-mediating cells that can respond to affected tissues or pathogens; therefore, they are a crucial population that reacts to diseases, including cancer, to protect the host.

Whereas the host responds to lesions in the body, the blood reveals consequent characteristic manifestations—*i.e.*, neutrophilia for bacterial infection [4] or leukopenia for viral infection [5]. In the host with cancer, circulating blood contains characteristic immune-mediating cells—*e.g.*, cytotoxic T cells [6,7] and regulatory T cells [8,9]—due to the immune response to the disease. Assessment of these immune-mediating cells in blood is useful for evaluations of prognosis and therapeutic effect because cytotoxic T cells play a role in cancer eradication, whereas regulatory T cells inhibit the host anti-cancer immune response. Therefore, assessment of blood cells is a useful approach to evaluating host immune status in various diseases, including cancer [10,11].

Whole-genome expression analysis using DNA microarray technology allows examination of various biological processes [12–14]. We have reported previously that peripheral blood exhibited a characteristic gene expression profile in cancer [15,16]. Although these studies suggest the usefulness of peripheral blood gene-expression analysis for exploration of the pathophysiological features/conditions of cancer, how the altered gene expression profile of blood cells contributes to understanding of the condition of individuals with cancer remains unknown.

We have established subcutaneous hepatocellular carcinoma (HCC) murine models that show the unique course of cancer: transient development followed by diminishing. This course was mediated by the immune response, particularly CD4+ T cells. Altered gene expression in whole blood cells as well as local

Abbreviation: HCC, hepatocellular carcinoma.

* Corresponding author. Address: Department of Gastroenterology, Kanazawa University, 13-1 Takara-machi, Kanazawa, Ishikawa 920-8641, Japan. Fax: +81 76 234 4250.
E-mail address: skaneko@m-kanazawa.jp (S. Kaneko).

0006-291X/$ - see front matter © 2012 Elsevier Inc. All rights reserved.
http://dx.doi.org/10.1016/j.bbrc.2012.10.004

tumor-associated inflammatory cells implied CD4+ T cell-involvement. Furthermore, the gene expression profiles of blood differed depending on the condition of cancer tissues, suggesting that blood-cell gene expression is associated with tumor condition and that its analysis is useful for investigation of the biological features of the host immune response to cancer.

2. Materials and methods

2.1. Cell culture

Hepa1-6 (ATCC, Manassas, VA), an established murine HCC cell line, was maintained in Dulbecco's modified Eagle's medium (Life Technologies, Carlsbad, CA) supplemented with 10% heat-inactivated fetal bovine serum (Life Technologies).

2.2. Subcutaneous HCC murine model

C57Bl/6 female mice (8 weeks old; Charles River Laboratories, Yokohama, Japan) or BALB/c athymic female mice (8 weeks old) were injected subcutaneously with 1×10^7 Hepa1-6 cells. Tumor size was monitored and the volume was calculated using the following formula:

$$\text{Tumor volume}(\text{mm}^3) = (\text{the shortest diameter})^2 \times (\text{the longest diameter})/2$$

Animal experiments were approved by the institutional review board.

2.3. Immunohistochemistry

Hepa1-6 subcutaneous tumor tissues were removed and embedded in optimal cutting temperature compound (Sakura Finetek, Torrance, CA), snap-frozen in liquid nitrogen, and cryostat-sectioned. Tissues were also fixed with neutral-buffered formalin, embedded in paraffin, cut into 4-μm sections, mounted on microscope slides, and stained with hematoxylin and eosin. Cryostat sections of frozen tissues were fixed in cold acetone, and endogenous biotin/avidin in the tissue specimens were blocked using a blocking kit (Vector Laboratories, Inc., Burlingame, CA). Slides were incubated with the appropriately diluted primary antibodies, anti-mouse CD4, CD8, CD11b (BD Pharmingen, Sparks, MD), and Gr-1 (eBioscience, San Diego, CA), respectively. The reactions were visualized using EnVision kits (DAKO, Glostrup, Denmark), followed by counterstaining with hematoxylin.

2.4. RNA isolation

Blood was obtained by retro-orbital venipuncture from mice and immediately stored as RNAlater aliquots (Ambion, Austin, TX). Total RNA of the obtained whole blood was extracted using the Mouse RiboPure™-Blood RNA Isolation Kit (Ambion), according to the manufacturer's protocol. A portion of Hepa1-6 tumor tissues was obtained and stored in RNAlater, followed by RNA isolation using the RNeasy Mini Kit (QIAGEN, Tokyo, Japan). The tumor fraction enriched with tumor-associated inflammatory cells was obtained using Histopaque®. Briefly, tumor tissues were minced and overlaid on the Histopaque® aliquot. After centrifugation, the visible separated monolayer was collected. RNA was isolated from the collected fraction using the microRNA Isolation Kit (Stratagene, La Jolla, CA), according to the manufacturer's protocol. The quality of purified RNA was analyzed using an Agilent 2100 Bioanalyzer (Agilent Technologies, Santa Clara, CA).

2.5. Gene expression analysis by DNA microarray and data analysis

Isolated RNA was amplified and labeled with Cy5 using the Quick Amp Labeling Kit (Agilent Technologies) according to the manufacturer's protocol. For reference, RNA isolated from the blood of normal C57Bl/6 or BALB/c athymic female mice was amplified and labeled with Cy3. The labeled objective and reference cRNA was mixed and hybridized using the Whole Mouse Genome 4×44K Array kit (Agilent Technologies). The slide was scanned using a DNA Microarray Scanner (Model G2505B; Agilent Technologies). Microarray data were deposited in NBCI Gene Expression Omnibus (GSE ID: GSE 39075).

Gene expression analysis was performed using the GeneSpring analysis software (Agilent Technologies). Each measurement was divided by the 75th percentile of all measurements in that sample at per chip normalization. Hierarchical clustering and principal component analysis of gene expression were performed. Welch's *t*-test with Benjamini and Hochberg's false discovery rate were used to identify genes that were differentially expressed in the groups of interest. Analysis of biological processes and networks was performed using the MetaCore software suite (GeneGo, Carlsbad, CA).

3. Results

3.1. Subcutaneous Hepa1-6 HCC cells in C57Bl/6 mice grew transiently and subsequently diminished due to the T-cell immune response

Hepa1-6 murine HCC cells were subcutaneously injected into C57Bl/6 female mice and tumor size was monitored. Until day 10, implanted Hepa1-6 cells proliferated continuously, forming a consistent tumor. From days 10 to 15, tumor size started to decrease, and the established tumors were completely eradicated by day 25 (Fig. 1A). In contrast, when Hepa1-6 cells were subcutaneously injected into BALB/c athymic mice, which were deleted of most, if not all, T cells due to the lack of a thymus, tumor tissues were established and continued to grow during the 37-day observation period without stabilization or diminishment (Fig. 1B). Histologically, tumors in C57Bl/6 mice obtained on days 10 and 15 were filled with viable Hepa1-6 cells (Fig. 1C). Tumor tissues obtained on day 20 showed fibrous tissues with few viable Hepa1-6 cells (Fig. 1C). Immunohistochemical analysis of immune-mediating cells in tumors showed that a substantial number of CD4+ T cells were found on day 10, the frequency of which was reduced after day 15 (Fig. 1D). In contrast, fewer CD8+ T cells were detected during any phase (Fig. 1D). CD11b+ and Gr-1+ cells were observed during all tumor phases (Fig. 1D). We also examined infiltrating inflammatory cells in the Hepa1-6 tumors after 10 days' growth in athymic mice. In contrast to the intensively infiltrating CD4+ T cells in Hepa1-6 tumors in C57Bl/6 mice on day 10 (Fig. 1D), few CD4+ T cells and no CD8+ T cells were observed in Hepa1-6 tumors from athymic mice (Supplementary Fig. S1). CD11b+ cells were diffusely present and a substantial number of infiltrating Gr-1+ cells were found (Supplementary Fig. S1). These results suggest that the characteristic feature of the immune response in subcutaneous Hepa1-6 tumors of C57Bl/6 mice on day 10 was CD4+ T cell-involvement.

3.2. Gene expression profiles of Hepa1-6 tumors on days 10 and 15

Tumors established in C57Bl/6 on days 10 and 15 revealed a similar appearance microscopically (Fig. 1C), whereas more CD4+ T cells infiltrated into tumors on day 10 than on day 15. To compare the molecular biological features of tumors on days 10 ($n = 3$) and 15 ($n = 3$), we assessed gene expression profiles using

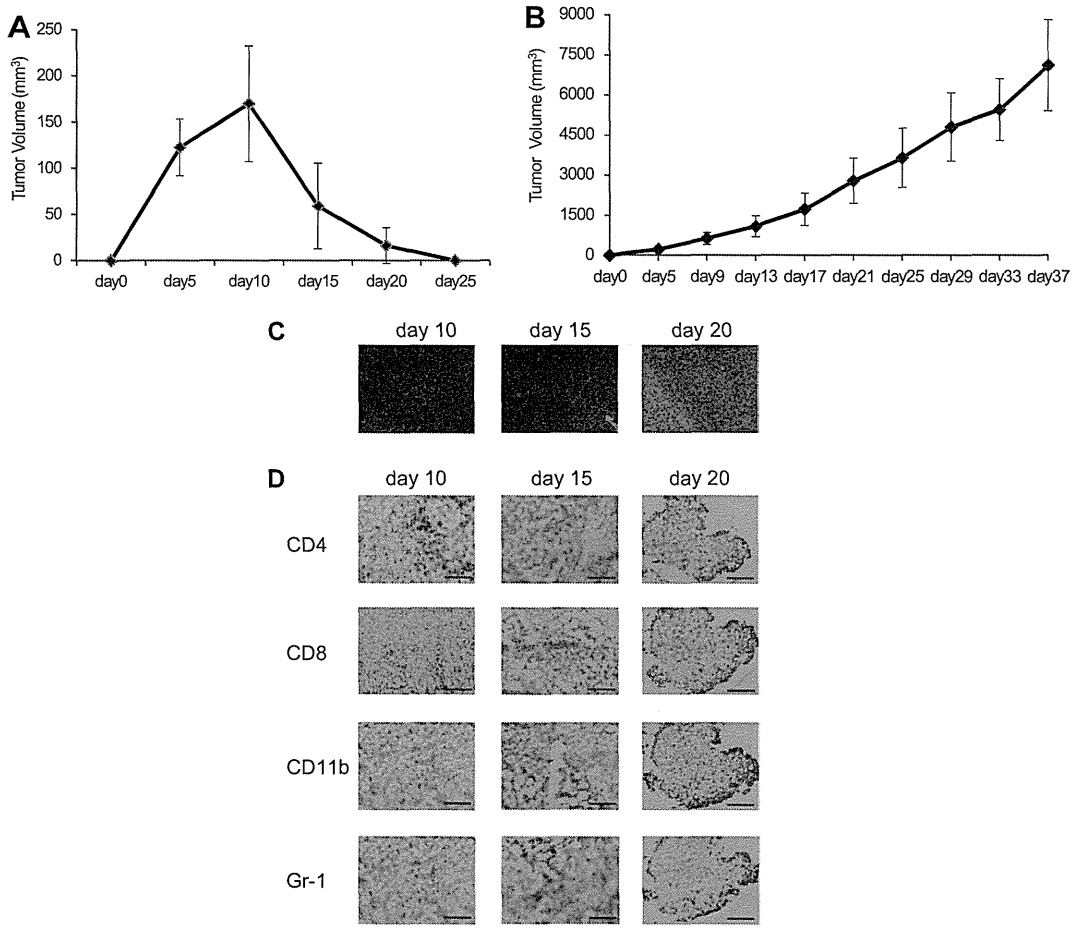

Fig. 1. The subcutaneous Hepa1-6 tumor model. Ten million Hepa1-6 HCC cells were subcutaneously inoculated into C57Bl/6 mice or Balb/c athymic mice. The size of tumors was monitored and tumor tissues were examined histologically as well as immunohistochemically. (A) Tumor growth in C57Bl/6 mice. (B) Tumor growth in Balb/c athymic mice. Bars, standard errors. (C) Histological features of inoculated Hepa1-6 subcutaneous tumors in C57Bl/6 mice on days 10, 15, and 25. Hematoxylin and eosin staining. Bars, 100 μm. (D) Immunohistochemical analysis of subcutaneous Hepa1-6 tumors in C57BL/6 mice on days 10, 15 and 25. Bars, 200 μm.

DNA microarrays. We identified 118 gene probes twofold differentially expressed between days 10 and 15 with $p < 0.05$ (Supplementary Table S1). Unsupervised hierarchical clustering and principal component analysis showed formation of two complete clusters on days 10 and 15 (Fig. 2). Network analysis of these 118 genes probes showed that regulation of T-cell proliferation was associated with the Stat5b, Stat5a, Jak2, Cyclin D1, and androgen receptor genes, whereas muscle filament sliding was associated with the Myh4, Myosin-IIA, Prelid2, Acta1, and Actc genes (Table 1). Thus, the T-cell immune responses to tumors on days 10 and 15 were markedly different.

3.3. Genes up-regulated in both blood and tumor-associated inflammatory cells were associated with local tumor conditions

The results shown above suggested that T cells, particularly CD4+ T cells, played an important role in the immune reaction to Hepa1-6 tumors in C57Bl/6 mice on day 10. To evaluate the relevance of local tumor inflammation and blood cells, we determined the genes whose expression was altered in the blood and tumor fraction enriched with tumor-associated inflammatory cells of C57Bl/6 mice ($n = 8$) or Balb/c athymic mice ($n = 3$) with Hepa1-6 tumors on day 10. We identified 127 genes whose expression was commonly twofold up-regulated ($p < 0.05$) between the tumor fraction enriched with tumor-associated inflammatory cells and whole blood cells in C57Bl/6 mice (Supplementary Table S2). The characteristic features involved a network that involved the C3g, IL-2r alpha chain, Shh, CD4, and Tgf-alpha genes (Table 2 and Fig. 3). Other networks were also observed to involve CD4: the network that involved Mkl2 (Mrtf-b), CD4, Dysstrophin, Pthr1, and Col1a2 and that involving CD4, Cdk1 (p34), iNOS, Tmem107, Dlx4 (Bp1). Sixty-five genes whose expression was commonly twofold up-regulated ($p < 0.05$) between the tumor fraction enriched with tumor-associated inflammatory cells and whole blood cells of athymic mice ($n = 3$) on day 10 were identified (Supplementary Table S3). Gene ontology processes for these genes included transcription, macromolecule metabolic process, regulation of multicellular organismal process, and development-related process, suggesting a role for local tumor-associated inflammatory cells in tumor development (Supplementary Table S4).

Thus, the biological features of genes up-regulated in both local tumor-associated inflammatory cells and blood cells suggested an underlying host CD4+ T cell-mediated immune response to tumors in C57Bl/6 mice, suggesting that the altered gene expression profile in systemically circulating blood cells reflected the local tumor conditions.

3.4. Whole peripheral-blood gene expression profiles were associated with tumor condition

Genes whose expression was altered in the blood of mice with Hepa1-6 tumors implied inflammation local to the tumor. We next

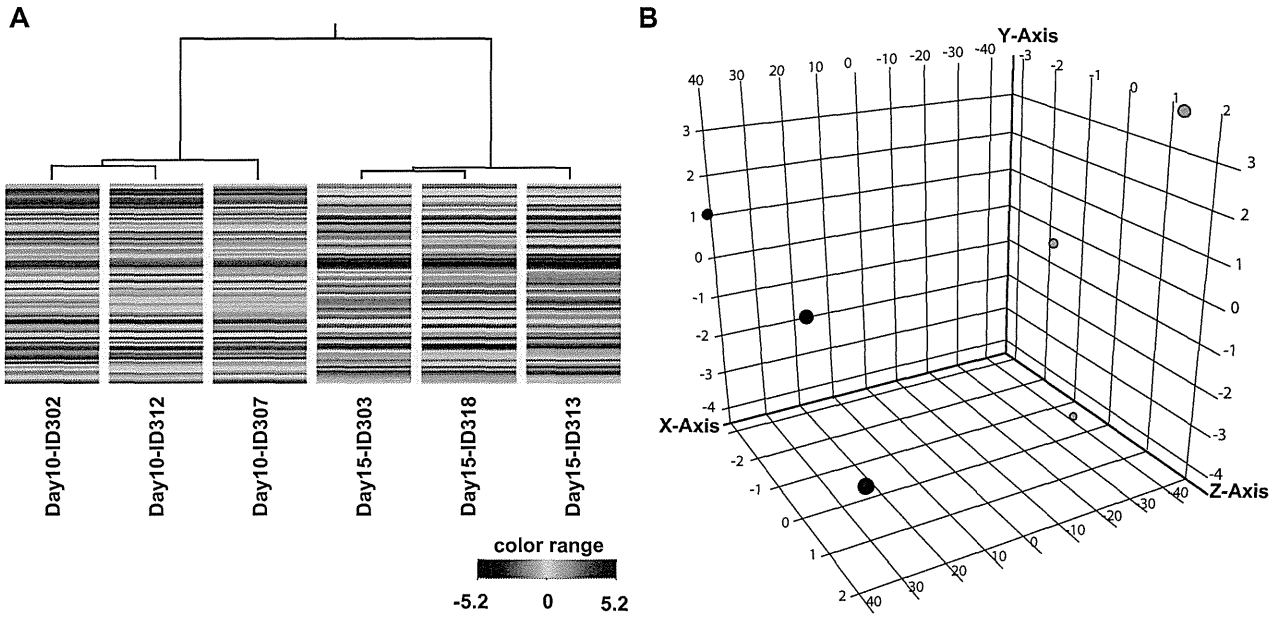

Fig. 2. Hierarchical clustering and principal component analysis of gene expression in subcutaneous Hepa1-6 tumors. Tumor tissues were obtained 10 and 15 days after subcutaneous inoculation of Hepa1-6 cells in C57Bl/6 mice and gene expression levels were evaluated by microarray. Unsupervised clustering (A) and principal component analysis (B) were performed using 118 probes specific for genes whose expression was significantly different at twofold. Filled circles, day 10. Gray circles, day 15.

Table 1
Networks for genes whose expression in tumors of C57Bl/6 mice was differetially expressed between day 10 and day 15.

Network	*p*-Value	GO processes
Stat5b, Androgen receptor, Stat5a, Jak2, Cyclin D1	0.0672	Positive regulation of activated T cell proliferation, cellular response to chemical stimulus, positive regulation of cell proliferation, regulation of activated T cell proliferation, response to hormone stimulus
Myh4, Myosin-IIA, Prelid2, Acta1, Actc	2.29×10^{-19}	Muscle filament sliding, actin-myosin filament sliding, actin-mediated cell contraction, actin filament-based movement, muscle system process
Rev-Eerb-b, Comp, Substance P receptor, Kcrm, Lingo1	7.02×10^{-15}	Regulation of multicellular organismal process, response to external stimulus, intracellular signal transduction, transmembrane receptor protein tyrosine kinase signaling pathway, multicellular organismal process
Bmal1, Stat5b, Pdgf-r-alpha, CD20, Dbp	7.26×10^{-13}	Positive regulation of transcription from RNA polymerase II promoter, regulation of transcription from RNA polymerase II promoter, positive regulation of gene expression, positive regulation of transcription, DNA-dependent, regulation of cellular biosynthetic process
Krt25, Keratin, type I cytoskeletal 25	0.00145	Intermediate filament organization, hair follicle morphogenesis, intermediate filament cytoskeleton organization, intermediate filament-based process, epidermis morphogenesis

explored how the gene expression profiles of whole blood cells changed with altering tumor conditions in mice with Hepa1-6 tumors. Blood was collected from C57Bl/6 mice before and 10, 15, 20, and 25 days after Hepa1-6 subcutaneous implantation, and then total RNA was isolated for gene expression analysis. The number of gene probes twofold up-regulated in the blood of mice with tumors compared with that of mice on day 0 was 968 on day 10 (Supplementary Table S5), 945 on day 15 (Supplementary Table S6), 53 on day 20 (Supplementary Table S7), and 14 on day 25 (Supplementary Table S8), and 418, 338, 61, and 134 gene probes, respectively, were down-regulated (Supplementary Tables S9, S10, S11 and S12). Unsupervised analysis of gene expression using 23,326 DNA microarray gene of that passed quality checking showed two major clusters, one associated with tumor presence on days 10, 15, and 20 (the tumor existence cluster), and the other to being tumor-free on days 0 and 25 (the tumor-free cluster), with minor discernible clusters depending on each day (Fig. 4A). Principal component analysis also revealed that the gene expression profile of each mouse differed depending on the day (Fig. 4B). We identified that 1525 genes probes was the union of 968 and 945 up-regulated genes probes on day 10 and day 15, indicating that 388 genes probes were commonly up-regulated. Despite considerable number of commonly up-regulated genes probes, clustering analysis using 1525 genes probes for gene expression profiles in blood on day 10 and day 15 formed two complete clusters discerning each day, suggesting that gene expression profile of blood was changing during the initiating phases of tumor diminishment. A pathway map analysis was performed on 968 and 945 genes whose expression was up-regulated on days 10 and 15, respectively. Development-related and cytoskeleton-remodeling pathways were the characteristic features of both groups (Supplementary Tables S13 and S14). Pathway maps for cell adhesion—integrin-mediated cell adhesion and migration, CCR4-induced leukocyte adhesion, plasmin signaling, and endothelial cell contacts by non-junctional mechanisms—were the prominent features of up-regulated genes on day 15 (Supplementary Table S14), suggesting enhanced involvement of tissue remodeling. We also analyzed the biological process features of genes differentially expressed between the tumor existence and tumor-free clusters. The number of gene probes whose expression was twofold up-regulated in the tumor existence cluster ($p < 0.05$) was 673, whereas 17 gene probes were down-regulated. The characteristic biological process networks indicated by these 673 gene probes were cytoskeleton, development, cell cycle, apoptosis, and cell adhesion (Supplemen-

Table 2
Networks for genes whose expression was commonly up-regulated in the tumor fraction enriched with tumor-associated inflammatory cells and blood of C57Bl/6 mice on day 10.

Network	*p*-Value	Gene ontology processes
C3g, Il-2r alpha chain, Shh, CD4, Tgf-alpha	9.26×10^{-22}	Positive regulation of cell proliferation, regulation of macromolecule metabolic process, cell proliferation, positive regulation of cellular process, regulation of cell proliferation
Cdk1 (p34), Aggrecan, Sox9, PNPase(old-35), Nyd-sp26	3.85×10^{-17}	Regulation of cell proliferation, generation of neurons, cellular developmental process, anatomical structure morphogenesis, neurogenesis
Nanos2, Nanos homolog 2	0.00143	Germ-line stem cell maintenance, negative regulation of meiosis, regulation of meiosis, regulation of meiotic cell cycle, stem cell maintenance
Wdr59, WD repeat-containing protein 59,	0.00143	Biological_process
Cdk1 (p34), Alk, Racgap1, Fibrinogen beta, Mmd	9.51×10^{-11}	Blood coagulation, coagulation, hemostasis, cytoskeleton organization, wound healing
Mkl2(Mrtf-b), CD4, Dystrophin, Pthr1, Col1a2	9.51×10^{-11}	Positive regulation of protein metabolic process, positive regulation of cellular metabolic process, positive regulation of metabolic process, regulation of cell proliferation, positive regulation of cellular process
Dnah12, Dynein, axonemal, heavy chains	0.00286	Microtubule-based movement, ATP catabolic process, ATP metabolic process, microtubule-based process, purine ribonucleoside triphosphate catabolic process
CD4, Cdk1 (p34), iNOS, Tmem107, Dlx4 (Bp1)	9.63×10^{-9}	Positive regulation of cellular metabolic process, interspecies interaction between organisms, positive regulation of metabolic process, positive regulation of macromolecule metabolic process, positive regulation of developmental process
Cdk1 (p34), Pthr1, Centg2, Bex2, Bex1	1.07×10^{-8}	G-protein signaling, coupled to cAMP nucleotide second messenger, cAMP-mediated signaling, G-protein signaling, coupled to cyclic nucleotide second messenger, cyclic-nucleotide-mediated signaling, regulation of catalytic activity
Fam33a, Mkl2(Mrtf-b), Cdk1 (p34), Tank, Pitx2	1.07×10^{-8}	Positive regulation of macromolecule metabolic process, positive regulation of cellular metabolic process, regulation of cellular metabolic process, cell cycle, positive regulation of metabolic process

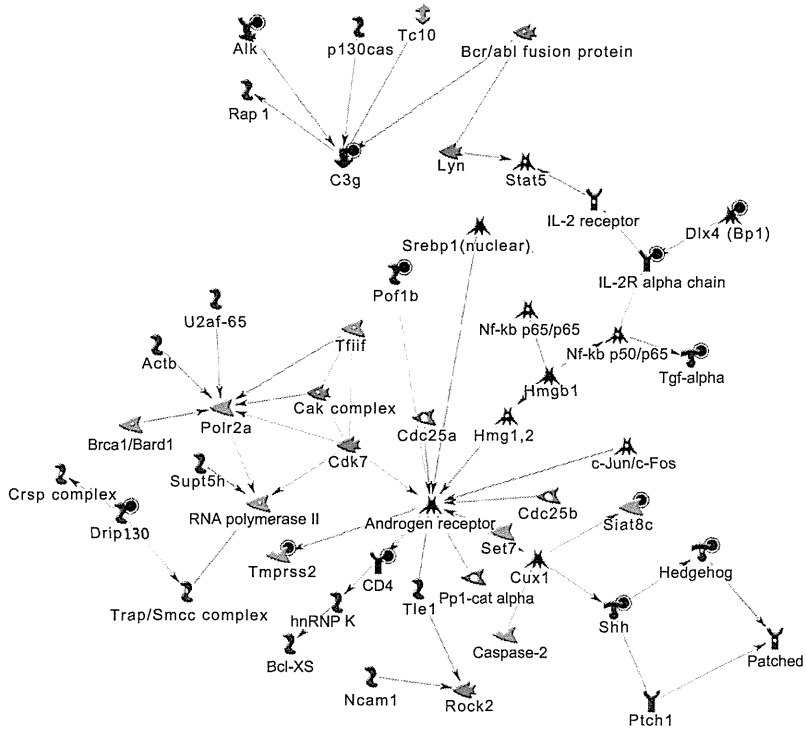

Fig. 3. Network depicting the involvement of C3G, IL-2R alpha chain, SHH, CD4, and TGF-alpha genes. Ten million Hepa1-6 cells were subcutaneously inoculated in C57Bl/6 mice. Blood and tumor tissues were obtained on day 10. Gene expression levels in blood and the fraction enriched with tumor-associated inflammatory cells were assessed by DNA microarray. One-hundred and twenty-seven genes were commonly up-regulated at twofold in blood and the tumor fraction enriched with tumor-associated inflammatory cells, and were related to the gene network that consisted of C3G, IL-2R alpha chain, SHH, CD4, and TGF-alpha plus related genes.

tary Table S15), implying the dynamic role of blood cells in immobilization and cellular kinesis, indicative of tissue remodeling, of tumors associated with the active immune response of the C57Bl/6 mouse.

We also examined whole blood gene expression profiles of BALB/c athymic mice with Hepa1-6 tumors on day 10 compared with that before inoculation of Hepa1-6 cells. Unsupervised clustering analysis of gene expression using 15583 gene probes that passed quality checking showed two clusters, clearly distinguishing between the tumor-existence and tumor-free conditions (Supplementary Fig. S2A). Principal component analysis showed that the gene expression profiles on days 0 and 10 tended to gather depending on the day (Supplementary Fig. S2B). We found that expression of 962 gene probes was up-regulated on day 10 compared with day 0. Pathway map analysis of the 962 gene probes revealed cell kinetics involving transcription, the cell cycle, and cell

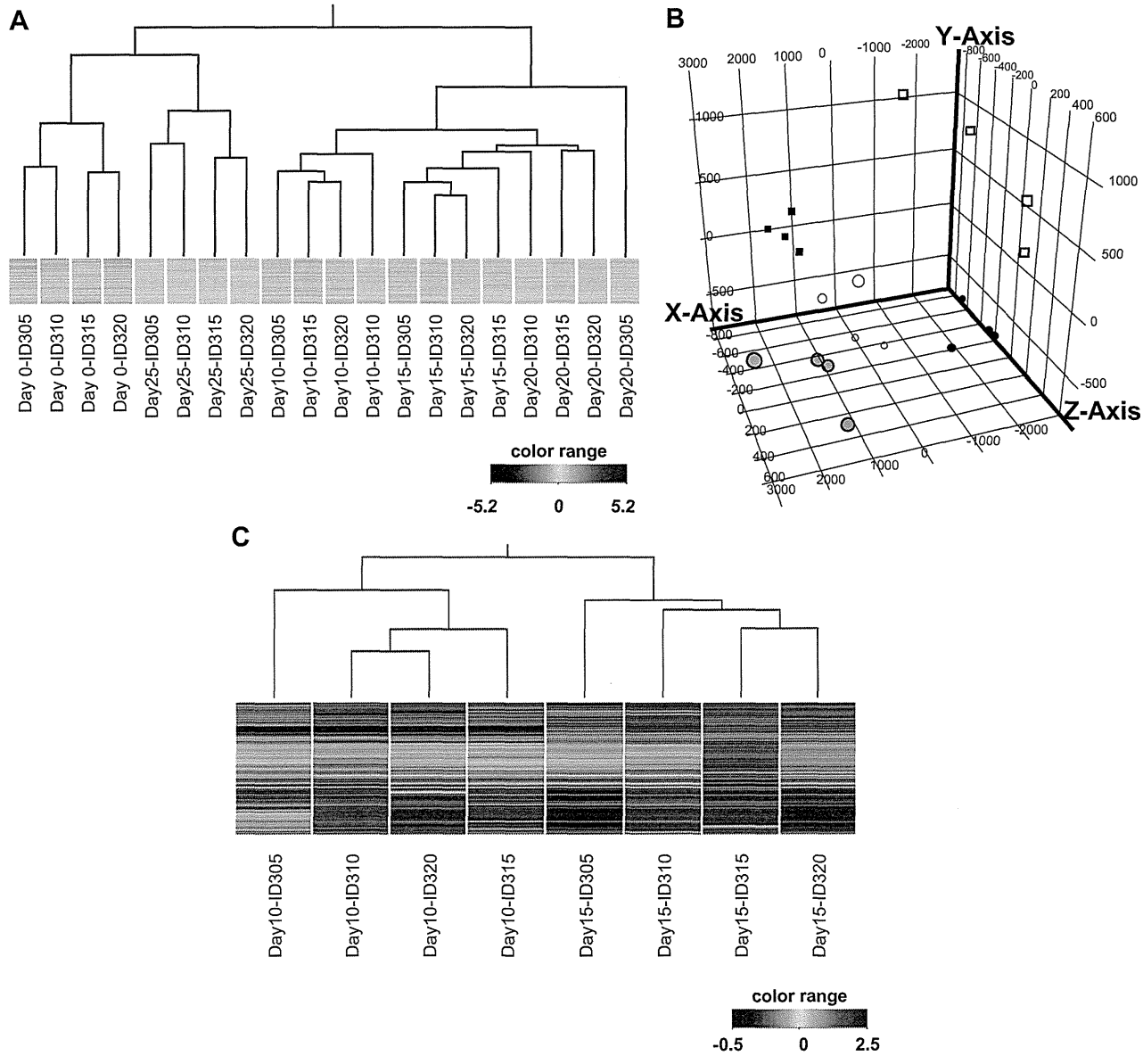

Fig. 4. Hierarchical clustering and principal component analysis of gene expression levels in blood obtained from C57Bl/6 mice inoculated subcutaneously with Hepa1-6 cells. RNA was extracted from the blood of C57Bl/6 mice inoculated with Hepa1-6 cells on days 0, 10, 15, 20, and 25, followed by gene expression analysis by DNA microarray. (A) Unsupervised hierarchical clustering and (B) principal component analysis of gene expression levels on day 0, 10, 15, 20, and 25 using all gene probes that passed a quality check. Open rectangle, day 0; filled rectangle, day 25; filled circle, day 10; gray circle, day 15; open circle, day 20. (C) Unsupervised hierarchical clustering of gene expression levels on day 10 and day 15 using the 1525 union genes probes up-regulated on day 10 and day 15.

adhesion (Supplementary Table S16), suggesting a relationship between blood cells and locally proliferating tumor cells that were inoculated subcutaneously. Thus, the gene expression profiles of whole blood cells in mice with tumors were altered depending on the local tumor conditions.

4. Discussion

The subcutaneously inoculated Hepa1-6 cells in C57Bl/6 mice demonstrated the unique course of tumor development/diminishment. Eradication of tumors was mediated by the T-cell immune response, particularly CD4+ T cells. Interestingly, genes up-regulated in both whole blood and the tumor fraction enriched with tumor-associated inflammatory cells on day 10 indicated a biological network involving CD4+ T cells, suggesting that gene expression alteration of whole blood cells was associated in part with the local inflammatory response to tumor tissues. Additionally, the gene expression profiles of whole blood cells in mice with Hepa1-6 tumors were associated with the tumor condition, and their biological features during tumor existence were suggestive of tissue remodeling-related processes.

The genes commonly affected in both blood cells and the tumor fraction enriched with tumor-associated inflammatory cells in C57Bl/6 mice suggested a biological network involving CD4+ T cells. Thus, CD4+ T cells may contribute to the altered blood gene expression profile on day 10. However, the blood gene expression profile of athymic mice with Hepa1-6 tumors was discernible from that of tumor-free mice, suggesting the involvement of other immune-mediating cells in the altered blood gene expression profile.

The gene expression profiles of whole blood cells of C57Bl/6 mice with tumors indicated biological processes related to tissue remodeling, such as development, cell adhesion, and the cytoskeleton. A fraction of circulating blood cells are involved in tissue remodeling/repair, such as monocytes/macrophages [17–19]. Thus, some blood cells likely contributed to these biological features as a consequence of tumor formation. The mechanism(s) underlying the association between blood gene expression profile and tumor condition should be determined.

We reported previously that features of the gene expression profile of peripheral blood mononuclear cells of HCC patients are shared with local inflammatory cells of HCC tissues [16]. In that analysis, the shared biological features were characterized by the local immune responses of the host to tumor tissues, tumor microenvironment—such as antigen presentation, response to hypoxia, and oxidative stress—ubiquitin-proteasomal proteolysis, mRNA processing, and the cell cycle. Peripheral blood mononuclear cells are devoid of cell types such as polymorphonuclear cells; therefore, the collected peripheral blood mononuclear cell populations rather contain inflammatory cells that are the major players in cancer immunity: the antigen-presenting cell population (monocytes/macrophages and dendritic cells), and the lymphocyte population (T and B cells) [20]. In the current study, gene expression of peripheral blood involved all cell populations therein. However, the genes up-regulated in both blood and the tumor fraction enriched with tumor-associated inflammatory cells suggested the importance of local tumor-associated CD4+ T cells, which played an important role in the C57Bl/6 mouse Hepa1-6 tumor model. Blood gene expression profiles of C57Bl/6 and athymic mice with Hepa1-6 tumors also depended on the presence and/or condition of a tumor. However, Gr-1+ cells were the major local inflammatory cells in the Hepa1-6 tumors of athymic mice. Because the network of genes up-regulated in blood and tumor-associated inflammatory cells in the athymic mouse model involved cellular kinetics and development, not directly suggestive of Gr-1+ cells, the role of local Gr-1+ cells in the alteration of blood gene expression profiles is unclear. Further studies should determine how immune-mediating cells in both blood and local tumor-infiltrating inflammatory cell populations alter blood gene expression depending on tumor condition.

The immune reaction of the host to cancer is complex: natural killer cells are well-characterized anti-cancer immune cells [21], and the innate immune system is represented by monocyte/macrophages [22]. In terms of acquired immunity, Th1 cells and cytotoxic T cells are known to be important due to the presence of antigen-presenting dendritic cells [23]. In contrast, the contradictory immune response is present concomitantly; this involves, for instance, regulatory T cells [8,9]. When anti-cancer immune cells predominate, cancer tissues will diminish. Conversely, when immune cells that work as suppressors of anti-cancer immunity are the major effectors, the tumor tissue will continue to grow. Thus, qualitative elucidation of host immune status is extremely important for assessing both prognosis and therapeutic efficacy. Blood gene expression analysis has been investigated extensively and has been shown to be useful in terms of diagnosis, prediction of a therapeutic effect, or prognosis in, for example, renal cell carcinoma [24], breast cancer [25], and digestive disease cancers [26]. Our data suggest that the blood gene expression profile of a murine cancer model was associated with the local tumor condition. The utility of blood cell gene expression profiling for further elucidation of the overall immune condition in terms of the presence of immune-mediating cell types should be investigated.

In conclusion, we observed that gene expression features of peripheral blood cells were altered depending on tumor condition. Additionally, biological features associated with CD4+ T cells, which play a pivotal role in Hepa1-6 C57Bl/6 tumor models, were implicated in the gene expression profiles common to both blood and tumor-infiltrating inflammatory cells. Further studies are needed to understand the systemic effect of cancer on blood gene expression profiles in other cancer-related conditions —*e.g.*, recurrent cancer or vaccination—for development of both novel diagnostic tools and effective treatments.

Acknowledgment

This work was supported in part by a subsidy of the Ministry of Education, Culture, Sports, Science and Technology, Japan.

Appendix A. Supplementary data

Supplementary data associated with this article can be found, in the online version, at http://dx.doi.org/10.1016/j.bbrc.2012.10.004.

References

[1] B.K. Edwards, E. Ward, B.A. Kohler, C. Eheman, A.G. Zauber, R.N. Anderson, A. Jemal, M.J. Schymura, I. Lansdorp-Vogelaar, L.C. Seeff, M. van Ballegooijen, S.L. Goede, L.A. Ries, Annual report to the nation on the status of cancer, 1975–2006, featuring colorectal cancer trends and impact of interventions (risk factors, screening, and treatment) to reduce future rates, Cancer 116 (2010) 544–573.
[2] S. De Masi, M.E. Tosti, A. Mele, Screening for hepatocellular carcinoma, Dig. Liver Dis. 37 (2005) 260–268.
[3] K. Nosho, Y. Baba, N. Tanaka, K. Shima, M. Hayashi, J.A. Meyerhardt, E. Giovannucci, G. Dranoff, C.S. Fuchs, S. Ogino, Tumour-infiltrating T-cell subsets, molecular changes in colorectal cancer, and prognosis: cohort study and literature review, J. Pathol. 222 (2010) 350–366.
[4] M.J. Delano, K.M. Kelly-Scumpia, T.C. Thayer, R.D. Winfield, P.O. Scumpia, A.G. Cuenca, P.B. Harrington, K.A. O'Malley, E. Warner, S. Gabrilovich, C.E. Mathews, D. Laface, P.G. Heyworth, R. Ramphal, R.M. Strieter, L.L. Moldawer, P.A. Efron, Neutrophil mobilization from the bone marrow during polymicrobial sepsis is dependent on CXCL12 signaling, J. Immunol. 187 (2011) 911–918.
[5] M.B. Edmonson, E.L. Riedesel, G.P. Williams, G.P. Demuri, Generalized petechial rashes in children during a parvovirus B19 outbreak, Pediatrics 125 (2010) e787–e792.
[6] L. Chen, Mimotopes of cytolytic T lymphocytes in cancer immunotherapy, Curr. Opin. Immunol. 11 (1999) 219–222.
[7] B. Weigelin, M. Krause, P. Friedl, Cytotoxic T lymphocyte migration and effector function in the tumor microenvironment, Immunol. Lett. 138 (2011) 19–21.
[8] S. Sakaguchi, Regulatory T cells: key controllers of immunologic self-tolerance, Cell 101 (2000) 455–458.
[9] E.M. Shevach, Mechanisms of foxp3+ T regulatory cell-mediated suppression, Immunity 30 (2009) 636–645.
[10] Y. Takata, Y. Nakamoto, A. Nakada, T. Terashima, F. Arihara, M. Kitahara, K. Kakinoki, K. Arai, T. Yamashita, Y. Sakai, E. Mizukoshi, S. Kaneko, Frequency of CD45RO+ subset in CD4 + CD25(high) regulatory T cells associated with progression of hepatocellular carcinoma, Cancer Lett. 307 (2011) 165–173.
[11] C. Yee, S.R. Riddell, P.D. Greenberg, *In vivo* tracking of tumor-specific T cells, Curr. Opin. Immunol. 13 (2001) 141–146.
[12] G.A. Churchill, Fundamentals of experimental design for cDNA microarrays, Nat. Genet. 32 (Suppl.) (2002) 490–495.
[13] C.J. Stoeckert Jr., H.C. Causton, C.A. Ball, Microarray databases: standards and ontologies, Nat. Genet. 32 (Suppl.) (2002) 469–473.
[14] J.S. Reis-Filho, L. Pusztai, Gene expression profiling in breast cancer: classification, prognostication, and prediction, Lancet 378 (2011) 1812–1823.
[15] M. Honda, Y. Sakai, T. Yamashita, A. Sakai, E. Mizukoshi, Y. Nakamoto, I. Tatsumi, Y. Miyazaki, H. Tanno, S. Kaneko, Differential gene expression profiling in blood from patients with digestive system cancers, Biochem. Biophys. Res. Commun. 400 (2010) 7–15.
[16] Y. Sakai, M. Honda, H. Fujinaga, I. Tatsumi, E. Mizukoshi, Y. Nakamoto, S. Kaneko, Common transcriptional signature of tumor-infiltrating mononuclear inflammatory cells and peripheral blood mononuclear cells in hepatocellular carcinoma patients, Cancer Res. 68 (2008) 10267–10279.
[17] J. Wyckoff, W. Wang, E.Y. Lin, Y. Wang, F. Pixley, E.R. Stanley, T. Graf, J.W. Pollard, J. Segall, J. Condeelis, A paracrine loop between tumor cells and macrophages is required for tumor cell migration in mammary tumors, Cancer Res. 64 (2004) 7022–7029.
[18] H.H. van Ravenswaay Claasen, P.M. Kluin, G.J. Fleuren, Tumor infiltrating cells in human cancer. On the possible role of CD16+ macrophages in antitumor cytotoxicity, Lab. Invest. 67 (1992) 166–174.
[19] R.D. Leek, K.L. Talks, F. Pezzella, H. Turley, L. Campo, N.S. Brown, R. Bicknell, M. Taylor, K.C. Gatter, A.L. Harris, Relation of hypoxia-inducible factor-2 alpha (HIF-2 alpha) expression in tumor-infiltrative macrophages to tumor angiogenesis and the oxidative thymidine phosphorylase pathway in human breast cancer, Cancer Res. 62 (2002) 1326–1329.

[20] J.E. Talmadge, Immune cell infiltration of primary and metastatic lesions: mechanisms and clinical impact, Semin. Cancer Biol. 21 (2011) 131–138.

[21] H. Kobayashi, S. Dubois, N. Sato, H. Sabzevari, Y. Sakai, T.A. Waldmann, Y. Tagaya, Role of trans-cellular IL-15 presentation in the activation of NK cell-mediated killing, which leads to enhanced tumor immunosurveillance, Blood 105 (2005) 721–727.

[22] P. Allavena, A. Mantovani, Immunology in the clinic review series; focus on cancer: tumour-associated macrophages: undisputed stars of the inflammatory tumour microenvironment, Clin. Exp. Immunol. 167 (2012) 195–205.

[23] S.J. Cronin, J.M. Penninger, From T-cell activation signals to signaling control of anti-cancer immunity, Immunol. Rev. 220 (2007) 151–168.

[24] N.C. Twine, J.A. Stover, B. Marshall, G. Dukart, M. Hidalgo, W. Stadler, T. Logan, J. Dutcher, G. Hudes, A.J. Dorner, D.K. Slonim, W.L. Trepicchio, M.E. Burczynski, Disease-associated expression profiles in peripheral blood mononuclear cells from patients with advanced renal cell carcinoma, Cancer Res. 63 (2003) 6069–6075.

[25] J. Aaroe, T. Lindahl, V. Dumeaux, S. Saebo, D. Tobin, N. Hagen, P. Skaane, A. Lonneborg, P. Sharma, A.L. Borresen-Dale, Gene expression profiling of peripheral blood cells for early detection of breast cancer, Breast Cancer Res. 12 (2010) R7.

[26] M.J. Baine, S. Chakraborty, L.M. Smith, K. Mallya, A.R. Sasson, R.E. Brand, S.K. Batra, Transcriptional profiling of peripheral blood mononuclear cells in pancreatic cancer patients identifies novel genes with potential diagnostic utility, PLoS One 6 (2011) e17014.

Published OnlineFirst May 31, 2012; DOI:10.1158/0008-5472.CAN-12-0028

AACR

Cancer Research

Acyclic Retinoid Targets Platelet-Derived Growth Factor Signaling in the Prevention of Hepatic Fibrosis and Hepatocellular Carcinoma Development

Hikari Okada, Masao Honda, Jean S. Campbell, et al.

Cancer Res 2012;72:4459-4471. Published OnlineFirst May 31, 2012.

Published OnlineFirst May 31, 2012; DOI:10.1158/0008-5472.CAN-12-0028

Therapeutics, Targets, and Chemical Biology

Cancer Research

Acyclic Retinoid Targets Platelet-Derived Growth Factor Signaling in the Prevention of Hepatic Fibrosis and Hepatocellular Carcinoma Development

Hikari Okada[1], Masao Honda[1,2], Jean S. Campbell[4], Yoshio Sakai[1], Taro Yamashita[1], Yuuki Takebuchi[1], Kazuhiro Hada[1], Takayoshi Shirasaki[1], Riuta Takabatake[1], Mikiko Nakamura[1], Hajime Sunagozaka[1], Takuji Tanaka[3], Nelson Fausto[4], and Shuichi Kaneko[1]

Abstract

Hepatocellular carcinoma (HCC) often develops in association with liver cirrhosis, and its high recurrence rate leads to poor patient prognosis. Although recent evidence suggests that peretinoin, a member of the acyclic retinoid family, may be an effective chemopreventive drug for HCC, published data about its effects on hepatic mesenchymal cells, such as stellate cells and endothelial cells, remain limited. Using a mouse model in which platelet-derived growth factor (PDGF)-C is overexpressed (*Pdgf-c Tg*), resulting in hepatic fibrosis, steatosis, and eventually, HCC development, we show that peretinoin significantly represses the development of hepatic fibrosis and tumors. Peretinoin inhibited the signaling pathways of fibrogenesis, angiogenesis, and Wnt/β-catenin in *Pdgf-c* transgenic mice. *In vitro*, peretinoin repressed the expression of PDGF receptors α/β in primary mouse hepatic stellate cells (HSC), hepatoma cells, fibroblasts, and endothelial cells. Peretinoin also inhibited PDGF-C–activated transformation of HSCs into myofibroblasts. Together, our findings show that PDGF signaling is a target of peretinoin in preventing the development of hepatic fibrosis and HCC. *Cancer Res; 72(17); 4459–71. ©2012 AACR.*

Introduction

Hepatocellular carcinoma (HCC) is one of the most common malignancies worldwide with a particularly poor patient outcome (1). It often develops as a result of chronic liver disease associated with hepatitis B or hepatitis C virus infection or with other etiologies such as long-term alcohol abuse, autoimmunity, and hemochromatosis (2–5). Despite the recent advances in antiviral therapy for hepatitis B or hepatitis C virus, these are insufficient to completely prevent the occurrence of HCC. Moreover, the recent increase in nonalcoholic fatty liver disease (NAFLD) associated with metabolic syndrome is a potential high-risk factor for the development of HCC (6).

HCC often develops during the advanced stages of liver fibrosis and is associated with deposits of extracellular matrix synthesized by activated stellate cells. During the course of chronic hepatitis, nonparenchymal cells, including Kupffer, endothelial, and activated stellate cells, release a variety of cytokines and growth factors. One of these growth factors is platelet-derived growth factor (PDGF), which is involved in fibrogenesis, angiogenesis, and tumorigenesis (7, 8). PDGF expression has been shown to be upregulated from the early stages of chronic hepatitis, suggesting its association with the development of fibrosis in chronic hepatitis C (CH-C; refs. 9 and 10). Overexpression of PDGF-C in mouse liver resulted in the progression of hepatic fibrosis, steatosis, and the development of HCC; this mouse model closely resembles the human HCC, which is frequently associated with hepatic fibrosis (7).

Peretinoin (generic name; code, NIK-333), developed by the Kowa Company, is an oral acyclic retinoid with a vitamin A–like structure, which targets the retinoid nuclear receptor. Oral administration of peretinoin was shown to significantly reduce the incidence of posttherapeutic HCC recurrence and improve the survival rates of patients in a clinical trial (11, 12). A large-scale clinical study including various countries is now planned to confirm its clinical efficacy.

Although peretinoin treatment can suppress HCC-derived cell line growth and inhibit experimental mouse or rat liver carcinogenesis (13, 14), the detailed mechanism of its effect has not been fully elucidated. Peretinoin has a high binding affinity to cellular retinoic acid-binding protein (15) and may interact with retinoic acid receptor-β and retinoid X receptor-α (16); however, the precise molecular targets for preventing HCC recurrence have not yet been elucidated.

Authors' Affiliations: [1]Department of Gastroenterology, Kanazawa University Graduate School of Medicine; [2]Department of Advanced Medical Technology, Kanazawa University Graduate School of Health Medicine; [3]Department of Oncologic Pathology, Kanazawa Medical University, Kanazawa, Japan; and [4]Department of Pathology, University of Washington School of Medicine, Seattle, Washington

Note: Supplementary data for this article are available at Cancer Research Online (http://cancerres.aacrjournals.org/).

Corresponding Author: Masao Honda, Department of Gastroenterology, Graduate School of Medicine, Kanazawa University, Takara-Machi 13-1, Kanazawa 920-8641, Japan. Phone: 81-76-265-2235; Fax: 81-76-234-4250; E-mail: mhonda@m-kanazawa.jp

doi: 10.1158/0008-5472.CAN-12-0028

Published OnlineFirst May 31, 2012; DOI:10.1158/0008-5472.CAN-12-0028

In this study, we used PDGF-C transgenic (*Pdgf-c* Tg) mice to show that PDGF-C signaling is a possible target of peretinoin in the prevention of hepatic fibrosis, angiogenesis, and the development of HCC.

Materials and Methods

Chemicals

The acyclic retinoid peretinoin (generic name; code, NIK-333) [(2E,4E,6E,10E)-3,7,11,15-tetramethyl-2,4,6,10,14-hexadecapentaenoic acid, C20H30O2, molecular weight 302.46 g/mol] was supplied by Kowa Company.

Animal studies

The generation and characterization of *Pdgf-c Tg* have been described previously (7). Wild-type and *Pdgf-c Tg* mice on a C57BL/6J background were maintained in a pathogen-free animal facility under a standard 12-hour/12-hour light/dark cycle. After weaning at week 4, male mice were randomly divided into the following 3 groups: (1) *Pdgf-c Tg* or wild-type (WT) mice given a basal diet (CRF-1, Charles River Laboratories Japan), (2) *Pdgf-c Tg* or WT mice given a 0.03% peretinoin-containing diet, (3) *Pdgf-c Tg* or WT mice given a 0.06% peretinoin-containing diet. Control mice were normal male homozygotes. At week 20, mice were sacrificed to analyze the progression of hepatic fibrosis ($n = 15$ for each of the 3 groups). At week 48, mice were sacrificed to analyze the development of hepatic tumors ($n = 31$ for the basal diet group, $n = 37$ for the 0.03% peretinoin group, and $n = 17$ for the 0.06% peretinoin group). The incidence of hepatic tumors, maximum tumor size, and liver weight were evaluated. None of the treated WT mice given a diet of 0.03% peretinoin died, but death occurred in 5% of WT mice around after 36 weeks of age receiving a 0.06% peretinoin diet, probably because of its toxicity. In *Pdgf-c Tg* mice, death was observed at similar frequency as WT mice that received 0.06% peretinoin diet.

All animal experiments were carried out in accordance with Guidelines for the Care and Use of Laboratory Animals at the Takara-Machi Campus of Kanazawa University, Japan.

Cell culture

Human HCC cell lines Huh-7, HepG2, and HLE, the mouse fibroblast cell line NIH3T3, human umbilical vein endothelial cells (HUVEC), and human stellate cells Lx-2 (kindly provided by Dr. Scott Friedman, Mount Sinai School of Medicine, New York, NY) were maintained in Dulbecco's Modified Eagle Medium (DMEM; Gibco) supplemented with 10% FBS (Gibco), 1% L-glutamine (Gibco), and 1% penicillin/streptomycin (Gibco) in a humidified atmosphere of 5% CO_2 at 37°C. 1 to 5×10^4 cells were seeded in each well of a 12-well plate the day before serum starvation in serum-free DMEM for 8 hours. The culture medium was then replaced with serum-free medium containing peretinoin. After 24-hour incubation, cells were harvested for analysis.

Isolation and culture of mouse hepatic stellate cells

Hepatic stellate cells (HSC) were isolated from C57BL/6J mice and the effect of recombinant human PDGF-C and peretinoin on HSCs was evaluated *in vitro*. Pronase-collagenase liver digestion was used to isolate HSC from wild-type mice. All experiments were replicated at least twice. Freshly isolated HSCs suspended in culture medium were seeded in uncoated 24-well plates and incubated at 37°C in a humidified atmosphere of 5% CO_2 for 72 hours. Nonadherent cells were removed with a pipette and the culture medium was replaced with medium containing 80 ng/mL recombinant human PDGF-C (Abnova) with or without peretinoin or 9-*cis*-retinoic acid (9cRA; 5 or 10 μmol/L). Cells were harvested for analysis after 24-hour incubation.

Isolation of peripheral blood mononuclear cells

Peripheral blood mononuclear cells were harvested and labeled with FITC-conjugate CD34 (Cell Lab) and R-Phycoerythrin (PE)-conjugated CD31 antibodies (Cell Lab) for 30 minutes at 4°C. After washing with 1 mL PBS, CD31 and CD34 surface expression was measured with a FACSCalibur flow cytometer (BD Biosciences). All flow cytometric data were analyzed using FlowJo software (Tree Star).

Gene expression profiling

Gene expression profiling in mouse liver was evaluated using the GeneChip Mouse Genome 430 2.0 Array (Affymetrix). Liver tissue from WT, *Pdgf-c Tg*, and *Pdgf-c Tg* with 0.06% peretinoin mice all at weeks 20 and 48 was obtained and a total of 34 chip assays were conducted as described previously (17). Expression data have been deposited in the Gene Expression Omnibus (GEO; NCBI Accession; GSE31431).

Pathway analysis was conducted using MetaCore (GeneGo). Functional ontology enrichment analysis was conducted to compare the Gene Ontology (GO) process distribution of differentially expressed genes ($P < 0.01$; refs. 10 and 17). Direct interactions among differentially expressed genes between *Pdgf-c Tg* mice with or without peretinoin administration were examined as reported previously (10). Each connection represents a direct, experimentally confirmed, physical interaction (MetaCore).

Histopathology and immunohistochemical staining

Mouse liver tissues were fixed in 10% formalin and stained with hematoxylin and eosin. The liver neoplasms (HCC and liver cell adenoma) were diagnosed according to previously described criteria (18, 19). Hepatic fibrosis was evaluated by Azan staining. Percentages of fibrous areas were calculated microscopically using an image analysis system (BIOREVO BZ-9000: KEYENCE Japan). Immunohistochemical (IHC) staining was conducted by an immunoperoxidase technique with an Envision kit (DAKO). Primary antibodies used were: rabbit polyclonal PDGFR-α (1:100 dilution), PDGFR-β (1:100 dilution), VEGFR1 (1:100 dilution), desmin (1:100 dilution), β-catenin (1:200 dilution), and mouse monoclonal cyclin D1 (1:400 dilution; all from Cell Signaling Technology); collagen 1 (1:100 dilution), collagen 4 (1:100 dilution), CD31 (1:100 dilution), and CD34 (1:100 dilution; all from Abcam, Cambridge, MA); and Tie-2 (1:80 dilution) and Myc (1:100 dilution; both from Santa Cruz Biotechnology).

Published OnlineFirst May 31, 2012; DOI:10.1158/0008-5472.CAN-12-0028

Quantitative real-time detection PCR

Total RNA was isolated from frozen liver tissue samples using a GenElute Mammalian Total RNA Miniprep Kit (Sigma-Aldrich) according to the manufacturer's protocol. cDNA was synthesized from 100 ng total RNA using a high-capacity cDNA reverse transcription kit (Applied Biosystems) then mixed with the TaqMan Universal Master Mix (Applied Biosystems) and each TaqMan probe. TaqMan probes used were PDGFR-α/β, VEGFR1/2, α-SMA, collagen 1/4, β-catenin, CyclinD1, and Myc (Applied Biosystems). Relative expression levels were calculated after normalization to glyceraldehyde-3-phosphate dehydrogenase (GAPDH).

Western blotting

Western blotting was conducted as described previously (20). Whole-cell lysates from mouse liver were prepared and lysed by CelLytic MT cell lysis reagent (Sigma-Aldrich) containing Complete Mini EDTA-free Protease Inhibitor cocktail tablets (Roche). Cytoplasmic and nuclear protein extracts were prepared using the NE-PER nuclear extraction reagent kit (Pierce Biotechnology). Primary antibodies used were PDGFR-α (1:1,000 dilution), PDGFR-β (1:1,000 dilution), VEGFR2 (1:1,000 dilution), p44/42 MAPK (1:1,000 dilution), total AKT (1:1,000 dilution), p-p44/42 MAPK (1:1,000 dilution), p-AKT (Ser473; 1:1,000 dilution), p-AKT (Thr308; 1:1,000 dilution), β-catenin (1:2,000 dilution), cyclin D1 (1:400 dilution), and lamin A/C (1:1,000 dilution; all Cell Signaling Technology); α-SMA (1:200 dilution; DAKO); 4-HNE (1:200 dilution; NOF); and GAPDH (1:1,000 dilution) and Myc (1:1,000 dilution; both Santa Cruz).

Statistical analysis

Results are expressed as mean ± SD. Significance was tested by 1-way analysis of variance with Bonferroni's method, and differences were considered statistically significant at $P < 0.05$.

Results

Peretinoin prevented the development of hepatic fibrosis in *Pdgf-c Tg*

To evaluate the HCC chemopreventive effects of peretinoin, we used a mouse model of *Pdgf-c Tg* in which PDGF-C is expressed under the control of the albumin promoter (7). Experimental mice were male mice expressing the PDGF-C transgene (*Pdgf-c Tg*); whereas male mice not expressing the transgene were considered WT. After weaning at week 4, *Pdgf-c Tg* or nontransgenic WT mice were fed a basal diet or a diet containing 0.03% or 0.06% peretinoin. At week 20, mice were sacrificed to analyze the progression of hepatic fibrosis. At week 48, mice were sacrificed to analyze the development of hepatic tumors (Fig. 1A). At week 20, Azan staining showed that predominant pericellular fibrosis had developed in *Pdgf-c Tg* mice (Fig. 1B). Densitometric analysis showed a significant dose-dependent reduction in the size of the fibrotic area in mice that received a diet containing peretinoin at both weeks 20 and 48 (Fig. 1C). Peretinoin therefore efficiently repressed the development of hepatic fibrosis in *Pdgf-c Tg* mice.

The expression of fibrosis-related genes in *Pdgf-c Tg* mice was evaluated by IHC staining, quantitative real-time detection PCR (RTD-PCR), and Western blotting. The expression of PDGFR-α and PDGFR-β, essential receptors for intracellular PDGF-C signaling, was upregulated mainly in the intracellular or portal area in *Pdgf-c Tg* mice livers (Fig. 2), but was significantly repressed by peretinoin after weaning at week 4. Similarly, the expression of collagen 1, collagen 4, and desmin was significantly upregulated in *Pdgf-c Tg* mice, but repressed by peretinoin (Fig. 2 and Supplementary Fig. S1A).

RTD-PCR results confirmed that these genes were substantially upregulated in *Pdgf-c Tg* mice and significantly repressed by both 0.03% and 0.06% peretinoin (Fig. 3A). Western blotting showed that the expression of phosphorylated extracellular signal-regulated kinase (p-ERK) 1/2 and cyclin D1, representative markers of the cell proliferation signaling pathway, was upregulated in *Pdgf-c Tg* mice, and repressed by peretinoin (Fig. 3B). Thus, peretinoin could partially but significantly prevent the development of hepatic fibrosis in *Pdgf-c Tg* mice during the study observation period of 48 weeks.

Peretinoin prevented the development of HCC in *Pdgf-c Tg* mice

At week 48, *Pdgf-c Tg* mice developed hepatic tumors with an incidence of 90% (Fig. 4A). Histologic assessment of these tumors verified that 54% (15/28) were adenomas and 46% (13/28) were HCC (Fig. 4A and C and Supplementary Fig. S2; ref. 21). Peretinoin (0.03%) dose-dependently repressed the incidence of hepatic tumors to 53% (19/36) and to 29% (5/17) at 0.06%. Correlating with tumor incidence, maximum tumor size and liver weight were also significantly repressed by peretinoin (Fig. 4B). Thus, peretinoin repressed the development of hepatic tumors in *Pdgf-c Tg* mice.

Serial gene expression profiling in the liver of *Pdgf-c Tg* mice that developed hepatic fibrosis and tumors

To examine which signaling pathways were altered during the progression of hepatic fibrosis and tumor development, we analyzed gene expression profiling in the liver of *Pdgf-c Tg* mice using Affymetrix gene chips. By filtering criteria for $P < 0.001$ and more than 2-fold differences, 538 genes were selected as differentially expressed. One-way hierarchical clustering analysis of differentially expressed genes is shown in Supplementary Fig. S3.

Of the 3 main clusters, 2 were upregulated (clusters A and B) and 1 was downregulated (cluster C). Cluster A consisted of immune-related [chemokine (C-C motif) receptor (CCR)4, CCR2, toll-like receptor (TLR)3 and TLR4], apoptosis-related [caspase (CASP)1 and CASP9], angiogenesis- and/or growth factor–related (PDGF-C, VEGF-C, osteopontin, HGF), oncogene-related [v-ets erythroblastosis virus E26 oncogene homologue (Ets)1, Ets2, CD44, N-myc downstream-regulated (NDRG)1], and fibrosis-related (tubulin) genes. The expression of cluster A genes was further upregulated in tumors at week

Published OnlineFirst May 31, 2012; DOI:10.1158/0008-5472.CAN-12-0028

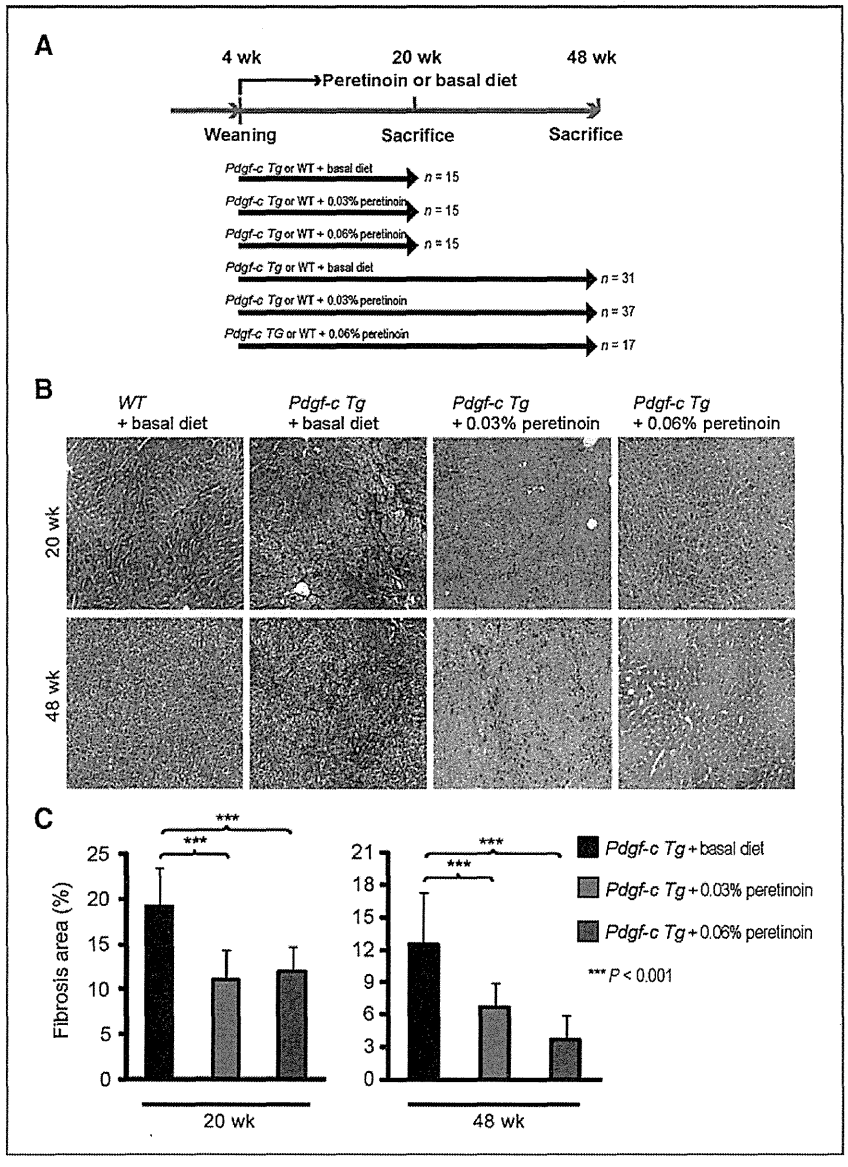

Figure 1. A, feeding schedule of *Pdgf-c Tg* and WT mice. After weaning, male mice were randomly divided into 3 groups: (i) *Pdgf-c Tg* or WT mice receiving basal diet, (ii) *Pdgf-c Tg* or WT mice receiving 0.03% peretinoin-containing diet, and (iii) *Pdgf-c Tg* or WT mice receiving 0.06% peretinoin-containing diet. B, Azan staining of WT or *Pdgf-c Tg* mouse livers fed with different diets at 20 weeks and 48 weeks. C, densitometric analysis of *Pdgf-c Tg* mouse liver fibrotic areas at 20 weeks ($n = 15$) and 48 weeks ($n = 15$).

48. Cluster B consisted mainly of connective tissue- and/or fibrosis-related [vascular cell adhesion molecule (VCAM)1, collagen I, III, IV, V, VI, integrin, decorin, TGF-βRII, PDGFR-α, and PDGFR-β] genes, the expression of which declined slightly at week 48. In contrast, cluster C, containing differentiation and liver function related genes [cytochrome P450, family 2, subfamily c (CYP2C)], were downregulated during the course of hepatic fibrosis and tumor development (Supplementary Fig. S4). Cluster C included xenobiotic- and metabolic process–related genes, which are potential targets of peretinoin. Peretinoin treatment prevented hepatic fibrosis and it preserved liver function. In addition, peretinoin might induce its target genes. Thus, peretinoin reduced the expression of upregulated genes (clusters A and B) and restored the expression of downregulated genes (cluster C) at both weeks 20 and 48 (Supplementary Figs. S3 and S4).

Published OnlineFirst May 31, 2012; DOI:10.1158/0008-5472.CAN-12-0028

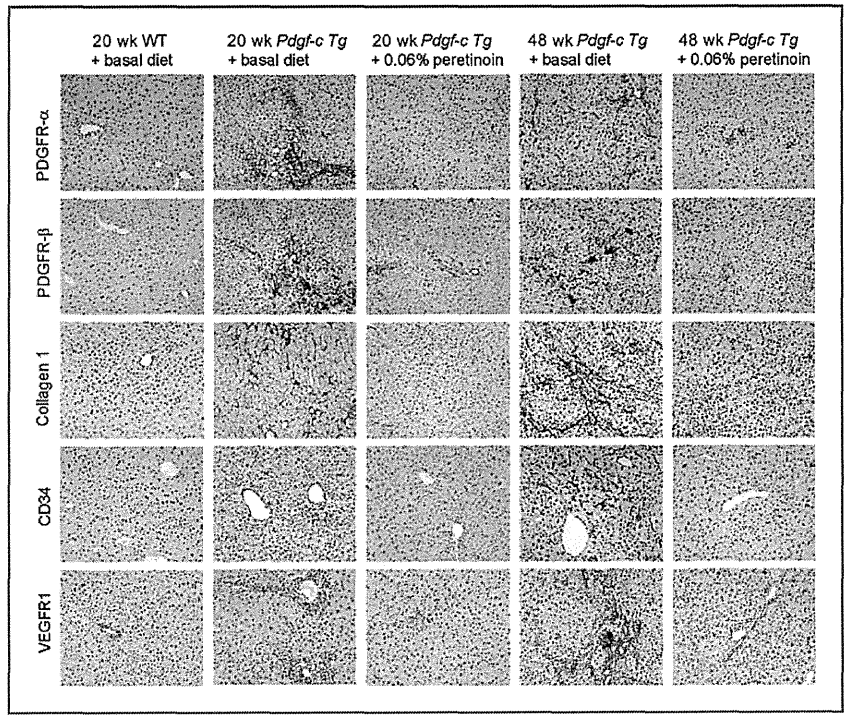

Figure 2. IHC staining of PDGFR-α, PDGFR-β, collagen 1, CD34, and VEGFR1 expression in *Pdgf-c Tg* or WT mouse livers fed a basal diet or 0.06% peretinoin.

To examine the molecular network consisting of differentially expressed genes in *Pdgf-c Tg* mice with or without peretinoin administration, the direct interactions of 513 genes were analyzed by MetaCore (i.e., 413 genes were downregulated and 100 genes were upregulated in *Pdgf-c Tg* mice treated with peretinoin compared with untreated mice; $P < 0.002$). A core gene network consisting of 41 genes was obtained (Supplementary Fig. S5) including interactions between representative growth factors, receptors (PDGFR and TGFβR), and transcriptional factors. Of these genes, the transcriptional factors Sp1 and Ap1 seem to be key regulators in the network (Supplementary Fig. S5).

Peretinoin inhibits PDGFR *in vitro*

Gene expression profiling landscaped the dynamic changes of signaling pathways in *Pdgf-c Tg* mice. To determine the effects of peretinoin *in vitro*, primary HSCs from normal C57BL/6J mice were stimulated by PDGF-C (Fig. 5) to induce the expression of PDGFR-α, PDGFR-β, alpha smooth muscle actin (α-SMA), and collagen 1a2; activated HSCs thus transformed into myofibroblasts (Fig. 5A and B). Peretinoin significantly reduced the expression of these genes and inhibited HSC activation.

We next evaluated the effects of peretinoin on human hepatoma cell lines (Huh-7, HepG2, and HLE), mouse embryonic fibroblast cells (NIH3T3), HUVECs, and Lx-2 (ref. 22; Supplementary Fig. S6A). Experimental conditions were optimized so that more than 90% of cells were variable at 20 μmol/L peretinoin, as determined by an MTS cell proliferation assay (data not shown). Peretinoin dose-dependently inhibited the expression of PDGFR-α and PDGFR-β in Huh-7, HepG2, HLE, NIH3T3, HUVEC, and Lx-2 cells, whereas no obvious expression of PDGFR-α was observed in HepG2 cells and HUVECs (Supplementary Fig. S6A). Peretinoin also inhibited VEGFR2 expression in HUVEC. These results were confirmed by RTD-PCR (data not shown). Correlating with these results, the expression of phosphorylated serine/threonine kinase AKT (p-AKT) and p-ERK1/2, downstream signaling molecules of PDGFR-α, PDGFR-β, and VEGFR2, was also dose-dependently repressed. The expression of collagen 1a2 was significantly repressed by peretinoin in Lx-2, HLE, and Huh-7 cells (Supplementary Fig. S6B). These results suggest that peretinoin may inhibit hepatic fibrosis, angiogenesis, and tumor growth through reduction of the PDGF and VEGF signaling pathway.

We examined the expression of 2 key regulators in peretinoin signaling, Sp1 and Ap1, in Huh-7 cells. Interestingly, the expression of Sp1 was decreased, which correlates with that of PDGFR-α, whereas expression of phosphorylated c-Jun (p-c-Jun) was increased in Huh-7 cells (Supplementary Fig. S6C). Therefore, peretinoin seems to repress the expression of PDGFR, partially through the inhibition of Sp1.

Peretinoin inhibits hepatic angiogenesis in *Pdgf-c Tg* mice

The effect of peretinoin on liver angiogenesis in *Pdgf-c Tg* mice was further analyzed. IHC staining of *Pdgf-c Tg* mouse

Published OnlineFirst May 31, 2012; DOI:10.1158/0008-5472.CAN-12-0028

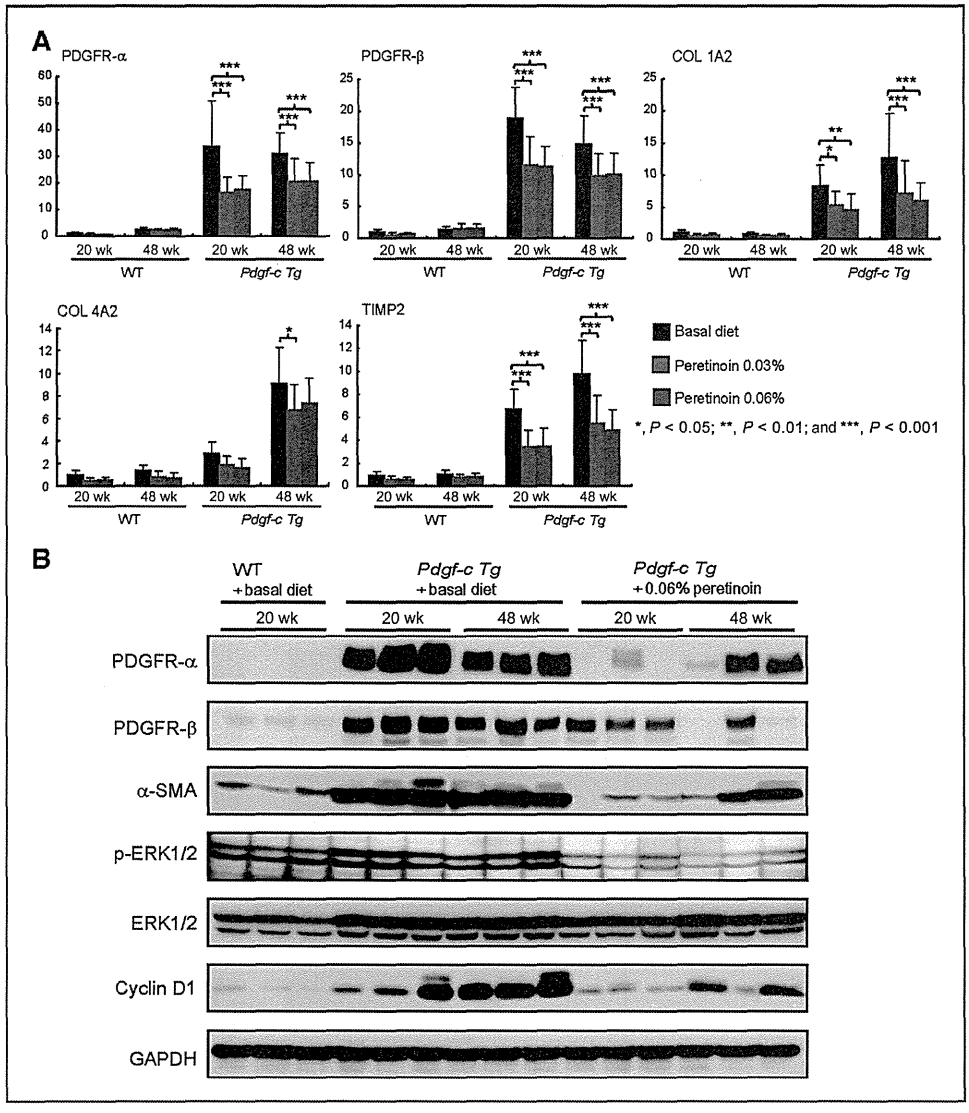

Figure 3. A, RTD-PCR analysis of PDGFR-α, PDGFR-β, collagen (COL) 1a2, collagen 4 a2, and TIMP2 expression in *Pdgf-c Tg* ($n = 5$) or WT mouse livers ($n = 15$). B, Western blotting of PDGFR-α, PDGFR-β, α-SMA, p-ERK, ERK, cyclin D1, and GAPDH expression in PDGF-C Tg or WT mouse livers fed a basal diet or 0.06% peretinoin at 20 or 48 weeks ($n = 3$).

livers at weeks 20 and 48 revealed overexpression of the endothelial markers CD31 and CD34 and the endothelial growth factors VEGFR1 and endothelium-specific receptor tyrosine kinase 2 (Tie2) in the mesenchymal region (Fig. 6 and Supplementary Fig. S1A). This expression was significantly repressed by peretinoin as determined by the densitometric area (Supplemental Fig. S1B). RTD-PCR results revealed significant upregulation of VEGFR1 (Flt-1) in *Pdgf-c Tg* mice compared with WT mice at both weeks 20 and 48, whereas the expression of VEGFR2 (Flk-1) and Tie2 was only upregulated at week 48. The expression of these genes was significantly repressed by peretinoin (Fig. 6A). Western blotting confirmed the upregulation of CD31 and VEGFR1 (Flk-1) at week 48 (Fig. 6B). In addition, p-AKT (Thr 308 and Ser 473) and 4-hydroxy-2-nonenal (4-HNE), an oxidative stress marker, were upregulated in *Pdgf-c Tg* mice and repressed by peretinoin (Fig. 6B).

We also assessed circulating endothelial cells (CEC), a useful biomarker for angiogenesis in the blood, and found that the $CD31^+/CD34^+$ CEC population was significantly upregulated in *Pdgf-c Tg* mice at week 48 but significantly repressed by peretinoin (Fig. 6C and D). Thus, peretinoin